# Composition and hygroscopicity of the Los Angeles Aerosol: CalNex

Scott P. Hersey,[1] Jill S. Craven,[1] Andrew R. Metcalf,[1,2] Jack Lin,[3] Terry Lathem,[3] Kaitlyn J. Suski,[4] John F. Cahill,[4] Hanh T. Duong,[5] Armin Sorooshian,[5] Haflidi H. Jonsson,[6] Manabu Shiraiwa,[1] Andreas Zuend,[1] Athanasios Nenes,[7] Kimberly A. Prather,[4] Richard C. Flagan,[1] and John H. Seinfeld[1]

Received 2 July 2012; revised 24 January 2013; accepted 21 February 2013; published 11 April 2013.

[1] Aircraft-based measurements of aerosol composition, either bulk or single-particle, and both subsaturated and supersaturated hygroscopicity were made in the Los Angeles Basin and its outflows during May 2010 during the CalNex field study. Aerosol composition evolves from source-rich areas in the western Basin to downwind sites in the eastern Basin, evidenced by transition from an external to internal mixture, as well as enhancements in organic O : C ratio, the amount of organics and nitrate internally mixed on almost all particle types, and coating thickness on refractory black carbon (rBC). Transport into hot, dilute outflow regions leads to significant volatilization of semivolatile material, resulting in a unimodal aerosol comprising primarily oxygenated, low-volatility, water-soluble organics and sulfate. The fraction of particles with rBC or soot cores is between 27 and 51% based on data from a Single Particle Soot Photometer (SP2) and Aerosol Time of Flight Mass Spectrometer (ATOFMS). Secondary organics appear to inhibit subsaturated water uptake in aged particles, while CCN activity is enhanced with photochemical age. A biomass-burning event resulted in suppression of subsaturated hygroscopicity but enhancement in CCN activity, suggesting that BB particles may be nonhygroscopic at subsaturated RH but are important sources of CCN. Aerosol aging and biomass burning can lead to discrepancies between subsaturated and supersaturated hygroscopicity that may be related to mixing state. In the cases of biomass burning aerosol and aged particles coated with secondary material, more than a single parameter representation of subsaturated hygroscopicity and CCN activity is needed.

**Citation:** Hersey, S. P., et al. (2013), Composition and hygroscopicity of the Los Angeles Aerosol: CalNex, *J. Geophys. Res. Atmos.*, *118*, 3016–3036, doi:10.1002/jgrd.50307.

## 1. Introduction

[2] Despite significant improvements in air quality resulting from decades of aggressive emission controls, annual $PM_{2.5}$ averages exceeded the national standard every year from 2000 to 2010 in the Los Angeles Basin [*AQMD*, 2012]. Several major coordinated studies have investigated air quality in Los Angeles, including the Southern California Air Quality Study (SCAQS) [*Eldering et al*., 1994; *Watson et al*., 1994; *Chow et al*., 1994; *Turpin and Huntzicker*, 1991], Southern California Ozone Study 1997 (SCOS97-NARSTO) [*Croes and Fujita*, 2003; *Liu et al*., 2000; *Pastor et al*., 2003; *Hughes et al*., 2002], Secondary Organic Aerosol in Riverside (SOAR) [*Docherty et al*., 2008; *Eatough et al*., 2008; *Denkenberger et al*., 2007], and Pasadena Aerosol Characterization Observatory (PACO) [*Hersey et al*., 2011; *Wonaschütz et al*., 2011]. The CalNex field study (http://www.esrl.noaa.gov/csd/calnex/), conducted from May to June 2010, was aimed at addressing both air quality and climate change through multi-agency collaboration to intensively sample gas and particulate pollutants from aircraft-, ship-, and ground-based platforms in both the San Joaquin Valley and Los Angeles Basin.

[3] A major fraction of aerosol mass in the Los Angeles Basin results from gas-phase oxidation of anthropogenic emissions, leading to condensation of secondary organics, sulfate, nitrate, and ammonium [*Docherty et al*., 2008], with primary black carbon (rBC or soot) particles serving as condensation sites for significant amounts of secondary

[1]California Institute of Technology, Pasadena, California, USA.
[2]Combustion Research Facility, Sandia National Laboratories, Livermore, California, USA.
[3]School of Earth and Atmospheric Sciences, Georgia Institute of Technology, Atlanta, Georgia, USA.
[4]University of California, San Diego, La Jolla, California, USA.
[5]University of Arizona, Tucson, Arizona, USA.
[6]Naval Postgraduate School, Monterey, California, USA.
[7]School of Earth and Atmospheric Sciences and School of Chemical and Biomolecular Engineering, Georgia Institute of Technology, Atlanta, Georgia, USA.

Corresponding author: J. H. Seinfeld, California Institute of Technology, Pasadena, CA, USA. (seinfeld@caltech.edu)


2169-897X/13/10.1002/jgrd.50307

material [*Pratt and Prather*, 2009; *Metcalf et al*., 2012]. The Basin may be characterized as source rich in the west, with prevailing W/SW winds transporting emissions primarily from motor vehicles, diesel engines, and shipping to downwind receptor sites in the east. Aerosols evolve during transport, leading to significant changes in composition and thereby affecting optical and physical properties of particles. As aerosol composition and mixing state evolve during downwind transport in the Los Angeles Basin, it is expected that subsaturated hygroscopicity and cloud condensation nuclei (CCN) properties of the aerosol likewise undergo changes. In the current study, we seek to understand (1) regional trends in aerosol composition in the Los Angeles Basin, (2) the characteristics of aging during downwind transport, (3) the impact of aerosol composition and evolution on both subsaturated and supersaturated aerosol hygroscopicity, and (4) the impact of biomass burning emissions on aerosol composition and hygroscopicity. Analysis is based on measurements made onboard the Center for Interdisciplinary Remotely Piloted Aircraft Studies (CIRPAS) Twin Otter aircraft during the CalNex field study during May 2010. With high time resolution measurements of composition from an Aerosol Time-of-Flight Mass Spectrometer (ATOFMS), Aerosol Mass Spectrometer (AMS), Single Particle Soot Photometer (SP2), Particle-into-Liquid Sampler with Total Organic Carbon (PILS-TOC), Differential Aerosol Sizing and Hygroscopicity Spectrometer Probe (DASH-SP), and Cloud Condensation Nuclei Counter (CCNC), we combine measurements of aerosol composition, mixing state, and subsaturated and supersaturated hygroscopicity in a single comprehensive study of aerosol characteristics in the Los Angeles Basin. The large area covered by measurements made onboard the Twin Otter (Figure 1) complements previous studies on aerosol composition and hygroscopicity at localized ground sites in the Los Angeles Basin and allows for direct characterization of evolution of the Los Angeles Aerosol during downwind transport.

## 2. Methods

### 2.1. CalNex Experiment

[4] The California Research at the Nexus of Air Quality and Climate Change (CalNex) experiment, conducted from May–July 2010 in the Los Angeles Basin and San Joaquin Valley, sought to address the impacts of anthropogenic pollutants on both air quality and climate change in California (www.esrl.noaa.gov/csd/calnex/). Sampling was conducted at two ground sites (Pasadena, CA, in the western Basin on the campus of the California Institute of Technology (34.1405°N, 118.1225°W), and near Bakersfield, CA, in the San Joaquin Valley (35.3463°N, 118.9654°W)), and onboard the Center for Interdisciplinary Remotely Piloted Aircraft Studies (CIRPAS; Naval Postgraduate School, Monterey, CA) Twin Otter aircraft, the NOAA Twin Otter aircraft, the NOAA WP-3D aircraft, the NASA King Air aircraft, and the NOAA R/V Ronald H. Brown.

[5] We report here on data collected onboard the CIRPAS Twin Otter aircraft over 18 flights during May 2010. *Metcalf et al*. [2012] outline CIRPAS Twin Otter flights in detail. The aircraft, hangared at the Ontario International Airport (Ontario, CA, USA), sampled extensively in the Los Angeles Basin, desert outflows, and southern San Joaquin Valley at an altitude of 300 m above ground level. Typical flight duration was 4 h and covered 700–800 km. We focus here on flights that circled the Los Angeles Basin and probed the outflow of the Los Angeles plume as it was transported through the Banning Pass in the eastern Basin. Regions of study in the Los Angeles Basin are identified in Figure 1, while *Metcalf et al*. [2012] show the entire CalNex study area, including the San Joaquin Valley, on a topographic map. A summary of the instruments sampling onboard the Twin Otter during CalNex, including the size ranges measured, is presented in *Metcalf et al*. [2012]. The operating dates for each instrument are described below, and mission averages described in the results refer to averages over the entire operating time of the respective instrument during CalNex. The ATOFMS

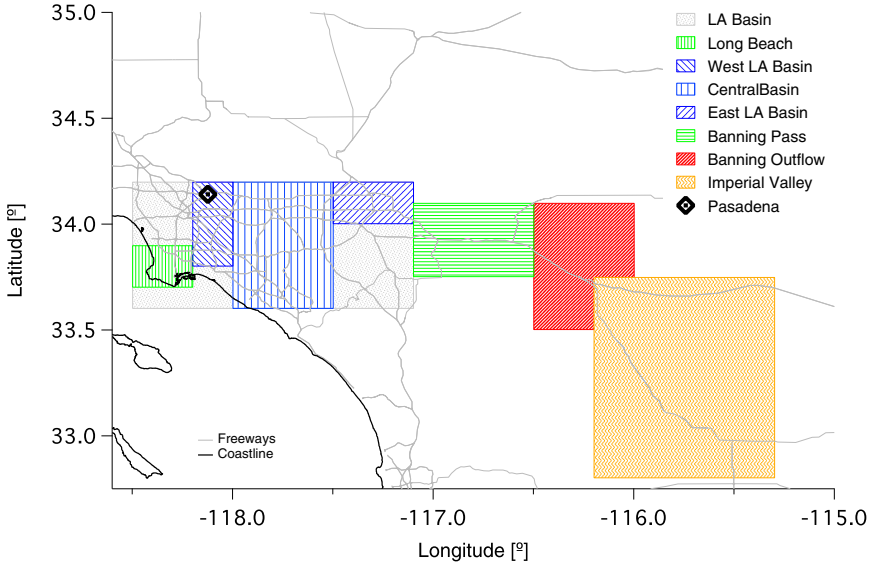


**Figure 1.** Definitions used in calculating regional averages of CalNex data. Only data below the boundary layer are included in analysis.

and AMS split time on the Twin Otter, which is why data are available for fewer days from those instruments. Gaps in data availability from other instruments indicate that instrument malfunction prevented collection of quality data.

### 2.2. Aerosol Mass Spectrometer (AMS)

[6] Chemical composition of submicrometer nonrefractory aerosol was measured with an Aerodyne compact Time-of-Flight Aerosol Mass Spectrometer (C-TOF-AMS; Aerodyne Research, Inc., Billerica, MA, USA) [*Jayne et al*., 2000; *Drewnick et al*., 2005; *Murphy et al*., 2009] during the final nine flights (18–22, 24–25, and 27–28 May 2010) onboard the CIRPAS Twin Otter. The instrument was operated in PTOF mode during five of those flights (21, 24–25, and 27–28 May 2010). Particles with vacuum aerodynamic diameters ($d_{va}$) 50 nm $\leq d_{va} \leq$ 800 nm, pass through a 2% chopper and are subsequently vaporized at 600°C. The chopper is operated in three modes, detecting background mass spectra, ensemble average mass spectra over all particle sizes, or size-resolved mass spectra. After vaporization, particles are ionized by 70 eV electron impact and pulsed orthogonally into a time-of-flight mass spectrometer. Mass spectral deconvolution resolves sulfate, nitrate, ammonium, chloride, and organic mass loadings. Approximate organic O : C ratios are calculated by using mass fraction of organic at *m/z* 44 to total organic and a parameterization presented by *Aiken et al*. [2008]. During CalNex, both bulk and size-resolved particle time-of-flight (PTOF) AMS data were collected and averaged to 1 min resolution. Comparison of PTOF-AMS to differential mobility analyzer (DMA; section 2.8) size distributions assumes density of 1.3 g $cm^{-3}$ for organics and 1.8 g $cm^{-3}$ for inorganic species.

### 2.3. Aerosol Time of Flight Mass Spectrometer (ATOFMS)

[7] Chemical characterization of individual aerosol particles was performed in situ using an aircraft-aerosol time-of-flight mass spectrometer (A-ATOFMS) [*Pratt et al*., 2009a] during the first five flights during CalNex (6–7, 10, and 14–15 May 2010). The A-ATOFMS uses an aerodynamic lens [*Liu et al*., 1995] to focus particles between 100 and 1000 nm. However, only particles with vacuum aerodynamic diameters between 100 and 300 nm were included in this analysis, to correspond to the size range of hygroscopicity measurements. The particles are aerodynamically sized by measuring the time it takes for the particle to pass through two 532 nm scattering lasers positioned a known distance apart. Particle speeds are converted to aerodynamic diameters using a calibration curve created with polystyrene latex spheres of known size. The sized particles are then desorbed and ionized using a pulsed 266 nm Nd-YAG laser. Positive and negative ion mass spectra from each particle are acquired using a dual polarity time-of-flight mass spectrometer. YAADA (www.yaada.org), a toolkit for Matlab (The MathWorks, Inc.), is used to facilitate data analysis. The mass spectra are clustered based on ion peak patterns and intensities using the ART-2a neural network [*Song et al*., 1999]. Clusters are then hand classified and grouped into particle types based on similar mass spectral characteristics. The ion peaks are labeled as the most probable ions based on previous source and laboratory studies at each mass-to-charge (*m/z*) ratio.

### 2.4. Single Particle Soot Photometer (SP2)

[8] Single-particle refractory black carbon (rBC) mass, as well as the thickness of coating that is nonrefractory at 4000K on each rBC particle, was measured by a Droplet Measurement Technologies (DMT; Boulder, CO, USA) Single Particle Soot Photometer (SP2) [*Stephens et al*., 2003; *Baumgardner et al*., 2004; *Schwarz et al*., 2006; *Moteki and Kondo*, 2007; *Slowik et al*., 2007] during 15 flights (6–7, 10, 12, 14–15, 18–22, 24–25, and 27–28 May 2010). In the SP2, rBC-containing particles are heated to their vaporization point as they pass through the active cavity of an Nd : YAG laser beam ($\lambda = 1064$ nm), with incandescence detected by two channels. Two scattering channels detect the scattering cross section of particles before incandescence, with Mie theory enabling determination of non-rBC coating thickness based on the scattering signal and the assumption of a core-shell morphology. *Metcalf et al*. [2012] details the calibration of this particular SP2 and the measurement techniques applied during Twin Otter flights. The rBC mass concentrations reported here are derived from lognormal fits to the single-particle size distributions, a correction which yields ~15–20% larger mass concentration than the raw data. The SP2 was calibrated with Aquadag (Aqueous Deflocculated Acheson Graphite; Acheson Colloids Company, Port Huron, MI, USA), which recently has been shown to yield calibration factors different than ambient soot would yield [*Baumgardner et al*., 2012; *Laborde et al*. 2012]. As reported by *Metcalf et al*. [2012], total rBC mass concentrations are ~12% smaller than comparable SP2s operated during CalNex. This potential bias has not been corrected for in the data presented here because the calibration standards have not yet been definitively linked to ambient rBC in the LA Basin. In addition, coating thickness diameters reported here may also be biased high, because each optical diameter may be assigned to a smaller rBC core particle. These potential biases will not change the spatio-temporal distribution of the measurements during CalNex.

[9] The refractory, light-absorbing fraction of combustion aerosol is referred to as either refractory black carbon (rBC) or soot, depending on whether it is detected by incandescence or thermochemical characteristics, respectively. The ATOFMS (section 2.3) identifies soot particles as those producing mass spectra with a simple carbon pattern often extending up to $C_{12}^{+}$ [*Moffet and Prather*, 2009]. In the SP2, particles, heated to their vaporization point, incandesce as they pass through a 1 MW Nd : YAG laser [*Schwarz et al*., 2006]. rBC particles are identified based on comparison of their ambient particle incandescence signature to those in laboratory-generated rBC particles. During CalNex, the number of soot particles detected by the ATOFMS was regionally correlated with rBC number concentration measured by the SP2, based on comparing time averages of data from each instrument over each region (Pearson's *R* correlation coefficient, *Pr*, equal to 0.91), and the two measurements are thus considered to provide similar estimates of the regional variability in soot-type combustion particles in Los Angeles. Nonetheless, for accuracy, rBC and soot will be defined, respectively, as the amount of light-absorbing material that incandesces with a signature that matches that of laboratory-generated rBC particles (rBC) and as the number of particles that produce mass spectral signature with simple carbon patterns (soot).

### 2.5. Particle-Into-Liquid Sampler With Total Organic Carbon (PILS-TOC)

[10] WSOC was quantified during 16 flights, using a particle-into-liquid sampler (PILS; Brechtel Manufacturing Inc.) coupled to a Total Organic Carbon (TOC) Analyzer (Sievers Model 800) [*Sullivan et al*., 2006; *Duong et al*., 2011], and data are presented here for 13 flights (6–7, 10, 12, 14–15, 18–21, 25, and 27–28 May 2010). Particles smaller than 2.5 μm in diameter are sampled by the PILS and passed immediately through an organic carbon denuder (Sunset Laboratory Inc.) to remove organic vapors. Particles are grown into droplets, collected by inertial impaction, and delivered through a 0.5 μm PEEK (polyetheretherketone) liquid filter prior to entering a TOC analyzer for quantification of WSOC approximately every 4 s. Reported WSOC concentrations represent the difference between the measured and background concentrations, which were obtained by passing sampled air through a high efficiency particulate air (HEPA) filter. The overall measurement uncertainty is estimated to be approximately 10%, with a minimum detection limit of 0.1 μg C $m^{-3}$. Synchronization of WSOC measurements with the other aircraft instrument data takes into account well-documented liquid transport delays in the PILS instrument [*Sorooshian et al*., 2006].

### 2.6. Differential Aerosol Sizing and Hygroscopicity Spectrometer Probe (DASH-SP)

[11] The Differential Aerosol Sizing and Hygroscopicity Spectrometer Probe (DASH-SP, Brechtel Mfg.) was used to measure subsaturated aerosol water uptake at 74 and 92% RH for 17 flights (4–7, 10, 12, 14–15, 18–22, 24–25, and 27–28 May 2010) during CalNex. The DASH-SP was operated as described by *Sorooshian et al*. [2008], except that the 85% RH humidification channel was not functioning. Ambient particles are dried in a nafion dryer before being size-selected in a cylindrical differential mobility analyzer (DMA) to generate a monodisperse aerosol of 150, 175, 200, or 225 nm dry diameter ($d_{dry}$) particles. After size selection, the flow of monodisperse aerosol is split into four separate flows, one providing a redundant measurement of particle number concentration via a condensation particle counter (CPC; TSI Model 3831), with the other three channels consisting of parallel nafion humidification chambers (Perma Pure, LLP, Model MD-070-24FS-4) operated at dry (< 10), 74, and 92% RH, followed by custom-built optical particle counters (OPCs). Within the OPCs, particles pass through a focused laser beam ($\lambda = 532$ nm; World Star Technologies, Model TECGL-30), where all forward-scattered light is collected and focused on a photomultiplier tube, and the resulting electrical pulse is recorded by a high-speed data acquisition computer. A dry refractive index is calculated from the dry OPC response to particles of known DMA size and used as an initial condition in an iterative data processing algorithm based on laboratory calibrations with salts of known refractive indices. The algorithm determines the best fit on a solution surface relating electrical pulse height, size, and refractive index, thereby accounting for the change in refractive index with particle water uptake. Temperature, pressure, and RH are monitored and controlled at several locations in the DASH-SP, ensuring that variability in these parameters does not impact growth factor measurements. RH was controlled to within 1.5%, and overall uncertainty in GF calculations is 4.5%.

[12] Two factors may result in volatilization of semivolatile species in the DASH-SP. First, sheath gas entering the DASH-SP is filtered through a Pall Life Sciences HEPA filter (p/n 12144). The large surface area of packing material is expected to effectively scrub the sheath gas of $NH_{3(g)}$, but is not expected to adsorb $HNO_{3(g)}$ or organic gases (personal correspondence with Pall), and is therefore expected to result in volatilization of $NH_4NO_3$. Next, utilization of a heating element to humidify DASH sample flows results in a temperature increase of 8°C between the aircraft inlet and DASH optical sizing, likely resulting in volatilization of both particulate $NH_4NO_3$ and semivolatile organics. Volatilization is expected to be modest, due to the short residence time in the DASH-SP (7 s total), but an explicit treatment of $NH_4NO_3$ volatilization and its effect on calculated water uptake of the organic fraction of particles is presented in section 3.4.

### 2.7. Scanning Flow Cloud Condensation Nuclei Analyzer (CCNC)

[13] CCN measurements were made with a Droplet Measurement Technologies streamwise, thermal-gradient cloud condensation nuclei counter (CCNC) [*Roberts and Nenes*, 2005; *Lance et al*., 2006] for 16 flights (5–7, 10, 12, 14–15, 18–22, 24–25, and 27–28 May 2010). Particles are introduced into the centerline of a cylindrical tube with wetted walls on which a streamwise, linear thermal gradient is applied. Owing to the difference in diffusivity between water and air molecules, a supersaturation is generated in the column, the maximum of which is located at the centerline. Particles that activate into cloud droplets are counted and sized with an optical particle counter.

[14] During CALNEX, the CCNC was operated as a CCN spectrometer using Scanning Flow CCN Analysis (SFCA) [*Moore and Nenes*, 2009]. In SFCA operation, dynamically changing the instrument flow while maintaining constant pressure and temperature gradients produces a nearly instantaneous change in supersaturation. The instrument temperature gradient was nominally held at 10K and the pressure maintained at 700 mb by use of a flow orifice and active flow control system, as described by *Moore et al*. [2011]. Nominal flow upscan and downscan times of 20 s were used.

[15] Instrument supersaturation was calibrated following the procedure in *Moore and Nenes* [2009]. Multiple calibrations were performed throughout the campaign to account for the effect of ambient temperature on the flow rate range. The uncertainty in CCNC supersaturation is estimated to be ± 0.04%. The uncertainty in CCN number concentration due to counting statistics and variations in temperature, pressure, and flow rates is estimated to be ~12% for CCN concentrations above 100 $cm^{-3}$ STP.

### 2.8. DMA Size Distributions

[16] Particle size distribution measurements were made with a cylindrical scanning differential mobility analyzer (TSI Model 3081) coupled to a condensation particle counter (TSI Model 3010) for 17 flights (4–7, 10, 12, 14–15, 18–22, 24–25, and 27–28 May 2010). An exponential scan from a mobility diameter of 10 nm to 800 nm is completed every 90 s. The sheath and excess flows of 2.5 l/min were used, with a 5 : 1 flow rate ratio of sheath-to-aerosol. The data are inverted following the method outlined by *Collins et al*. [2002], which corrects for the DMA transfer function

smearing as a result of a faster-than-normal scan time at a resolution of 5. Any residual smearing of the retrieved size distributions as a result of the operating parameters is expected to be minimal compared to the effect of sampling narrow plumes and changing air masses during flight.

## 3. Results and Discussion

### 3.1. Los Angeles Basin Meteorology

[17] Winds tend to display distinct and predictable diurnal patterns in the Los Angeles Basin [*Blumenthal et al*., 1978; *Lu and Turco*, 1995; *Hersey et al*., 2011]. Under the most frequent meteorology, stagnant or light offshore N/NE winds in the overnight hours (20:00–6:00 LT; UTC—8 h) give way to light onshore W/SW winds shortly after sunrise as surface heating generates a pressure gradient between cool coastal and warm inland areas. As solar heating intensifies through the day, the magnitude of the ocean-land pressure gradient increases and W/SW winds correspondingly increase in velocity to near 15 km/h by 15:00–16:00 LT. After 16:00 LT, winds decrease in velocity again to become stagnant, eventually changing direction as N/NE return flow increases in overnight hours. This local diurnal meteorology results in downwind transport of air from source-rich western portions of the Los Angeles Basin to receptor sites in the eastern Los Angeles Basin [*Lu and Turco*, 1995], with eventual transport out the El Cajon and Banning Passes and into desert outflow regions. Stagnant overnight winds can lead to pollutant buildup and carryover from one day to the next, resulting in an aged background aerosol in the Basin characterized by accumulation mode particles (0.1–1.0 μm diameter) containing a significant fraction of highly oxidized organic species [*Blumenthal et al*., 1978; *Hersey et al*., 2011]. *Metcalf et al*. [2012] found that meteorological conditions during May 2010 were more characteristic of springtime than classical summer meteorology in the Los Angeles Basin, but FLEXPART modeling of air parcel histories indicates similar air mass origin and west-east transport as described previously in Los Angeles. In general, spring meteorological conditions are characterized by similar overall patterns as the summer but generally weaker coast-land pressure gradients and onshore winds, cooler temperatures, and less intense photochemical conditions [*Hersey et al*., 2011]. Average ambient temperature (at flight altitude) over 18 flights during CalNex varied regionally, increasing from $16.1 \pm 2.0$°C in the western Basin to $18.3 \pm 3.4$°C in the eastern Basin and $24.3 \pm 1.8$°C in desert outflows (Figure 2k).

[18] Composition and hygroscopicity can vary spatially to a great extent within the Los Angeles Basin, and so discussion of trends will focus on averages over the sum of sampling hours for each respective instrument for each of 8 regions defined in Figure 1. The flight on 13 May 2010 was influenced by biomass burning emissions from a brush fire in the eastern Basin and will be considered separately.

### 3.2. Aerosol Bulk Composition

[19] Because diurnal wind patterns result in downwind transport of airborne species in the Los Angeles Basin, one may consider regional trends from west to east as representative of aerosol aging. Further aerosol aging between the Basin itself and outflow regions is expected to occur, as well as processes of dilution and volatilization. Analysis of bulk, nonrefractory, submicrometer aerosol composition from the AMS (average over nine flights: 18–22, 24–25, and 27–28 May 2010), SP2 (average over 15 flights: 6–7, 10, 12, 14–15, 18–22, 24–25, and 27–28 May 2010), and PILS-TOC (average over 13 flights: 6–7, 10, 12, 14–15, 18–21, 25, and 27–28 May 2010), with averages comprising total sampling hours for each instrument (Figures 2a–2k), will focus on regional, west-to-east trends in order to highlight aerosol evolution during downwind transport and aging. Black carbon characteristics are presented by *Metcalf et al*. [2012], and a detailed analysis of the organic fraction of aerosol (OA) by positive matrix factorization of AMS data will follow in a separate manuscript.

[20] Total submicrometer aerosol mass (Figure 2a), taken as the sum of non-refractory mass detected by the AMS and rBC mass detected by the SP2, displays distinct regional trends. Within the Los Angeles Basin, total submicrometer mass over May 2010 was relatively constant from west to east, averaging $7.7 \pm 3.9$ μg m$^{-3}$ in source-rich western areas and $8.2 \pm 4.6$ μg m$^{-3}$ in downwind eastern Basin receptor sites. This constant mass concentration was observed despite warmer temperatures in the eastern Basin (Figure 2k; $16.1 \pm 2.0$°C in the western Basin versus $18.3 \pm 3.4$°C in the eastern Basin) that are expected to lead to volatilization of semivolatile species and decreased aerosol mass. This suggests that as particles are transported downwind, secondary species are photochemically produced in the gas phase and condense onto particles. A sharp decrease in aerosol mass is observed from that in the Banning Pass ($4.9 \pm 3.8$ μg m$^{-3}$) to that in outflow regions ($1.2 \pm 0.2$ μg m$^{-3}$), as the Los Angeles plume is diluted upon transport into hot desert areas ($24.3 \pm 1.8$°C). Because there are no significant industrial sources of rBC in outflow areas and only one freeway in the region, rBC may be considered a conservative, nonvolatile tracer in outflow areas, and one may estimate the importance of volatilization by comparing the mass fraction of rBC (rBCMF; Figure 2g) in upwind versus downwind regions, according to the ratio:

$$rBC_{\text{Enhancement}} = \frac{rBCMF_{\text{Downwind}}}{rBCMF_{\text{Upwind}}}, \quad (1)$$

where $rBC_{\text{Enhancement}}$ is the enhancement in *rBCMF* between upwind ($rBCMF_{\text{Upwind}}$) and downwind ($rBCMF_{\text{Downwind}}$) sites. *rBCMF* is enhanced in outflow regions, and $rBC_{\text{Enhancement}}$ approaches 2.2 when comparing Basin aerosol with particles in outflows, underscoring the importance of volatilization during transport to outflows.

[21] Individual nonrefractory species exhibit behavior consistent with condensation of secondary material during downwind transport (Table 1 and Figures 2b–2f). The western Basin is characterized by relatively high sulfate and chloride mass fractions (SMF and CMF, respectively), owing to their marine sources and the highest concentration of shipping and industrial $SO_2$ emissions occurring in the western Basin and near Long Beach. The downwind eastern Basin is significantly enhanced in nitrate and ammonium mass fraction (NMF and AMF, respectively), compared to SMF and CMF, owing to photochemical production of nitrate during downwind transport and the presence of a large concentration of bovine $NH_3$ emissions in the area [*Neuman et al*., 2003; *Docherty et al*., 2008]. The local maximum in AMF in the

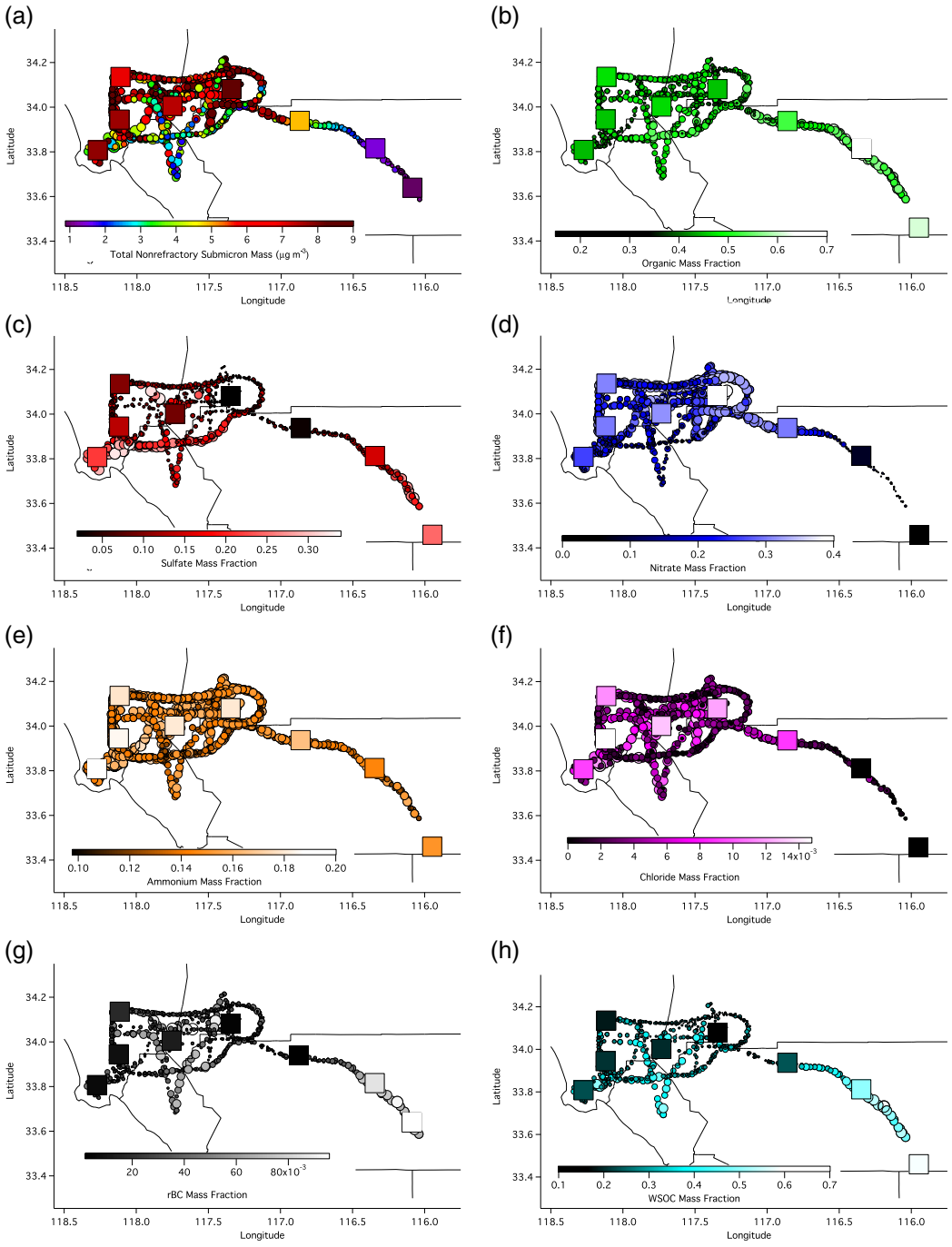


**Figure 2.** Bulk aerosol composition—regional trends from the AMS (average over nine flights: 18–22, 24–25, and 27–28 May 2010), SP2 (average over 15 flights: 6–7, 10, 12, 14–15, 18–22, 24–25, and 27–28 May 2010), and PILS-TOC (average over 13 flights: 6–7, 10, 12, 14–15, 18–21, 25, and 27–28 May 2010). Circles represent 1 min resolution data, while squares represent mission averages for the entirety of each instrument's operating period (sections 2.2) for each region. For clarity, color scales for mass fraction are different for each species. (a)Total mass, (b) organic mass fraction, (c) sulfate mass fraction, (d) nitrate mass fraction, (e) ammonium mass fraction, (f) chloride mass fraction, (g) refractive black carbon mass fraction, (h) wsoc mass fraction, (i) organic o:c ratio, (j) refractive black carbon coating thickness, and (k) surface temperature

Long Beach region may be associated with industrial selective catalytic reduction (SCR) and selective noncatalytic reduction (SNCR) $NO_x$ emission control strategies—both of which are associated with ammonia emissions [*Heck*, 1999]. Further, there are local maxima in sulfate mass in the Long Beach region, which would serve to drive ammonia into the particulate phase as $(NH_4)_2SO_4$ and $NH_4HSO_4$ and thereby enhance AMF relative to organics, nitrate, and chloride.

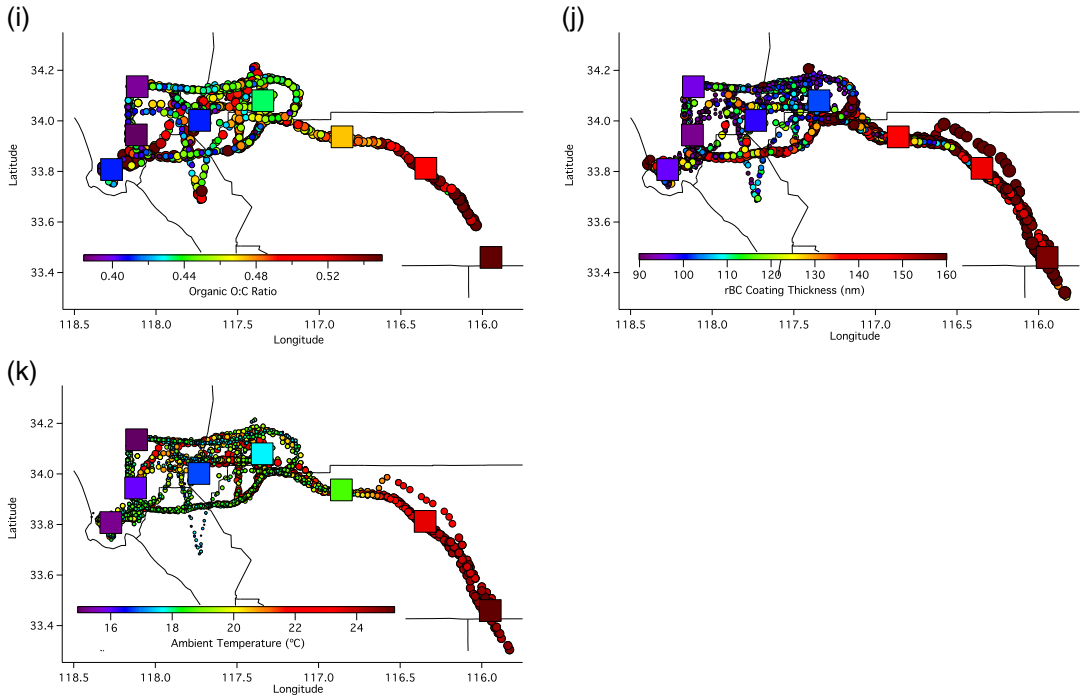


**Figure 2.** Continued

**Table 1.** Regional Averaged AMS Mass Concentrations and O : C Ratio for Nine Flights (18–22, 24–25, and 27–28 May 2010)

| | Total Aerosol Concentration [μg m$^{-3}$] | Organic Concentration [μg m$^{-3}$] | Sulfate Concentration [μg m$^{-3}$] | Nitrate Concentration [μg m$^{-3}$] | Ammonium Concentration [μg m$^{-3}$] | Chloride Concentration [μg m$^{-3}$] | Organic O : C Ratio |
|---|---|---|---|---|---|---|---|
| Long Beach | 7.81 (± 3.02) | 2.54 (± 0.74) | 1.33 (± 0.64) | 2.21 (± 1.36) | 1.49 (± 0.69) | 0.07 (± 0.06) | 0.41 (± 0.10) |
| West Basin | 7.71 (± 3.85) | 2.54 (± 0.99) | 0.92 (± 0.45) | 2.55 (± 2.04) | 1.42 (± 0.80) | 0.10 (± 0.07) | 0.38 (± 0.08) |
| Pasadena | 6.96 (± 4.33) | 2.38 (± 0.99) | 0.68 (± 0.29) | 2.41 (± 2.47) | 1.24 (± 0.93) | 0.08 (± 0.07) | 0.39 (± 0.07) |
| Central Basin | 7.44 (± 4.12) | 2.48 (± 0.99) | 0.63 (± 0.33) | 2.80 (± 2.39) | 1.35 (± 0.86) | 0.09 (± 0.08) | 0.41 (± 0.08) |
| East Basin | 8.24 (± 4.63) | 2.60 (± 0.99) | 0.43 (± 0.17) | 3.56 (± 2.77) | 1.48 (± 0.95) | 0.09 (± 0.08) | 0.43 (± 0.05) |
| Banning Pass | 4.90 (± 3.85) | 1.80 (± 0.75) | 0.23 (± 0.07) | 1.87 (± 2.09) | 0.84 (± 0.92) | 0.06 (± 0.07) | 0.47 (± 0.09) |
| Banning Outflow | 1.44 (± 0.36) | 0.91 (± 0.24) | 0.20 (± 0.08) | 0.12 (± 0.09) | 0.14 (± 0.11) | 0.00 (± 0.02) | 0.49 (± 0.09) |
| Imperial Valley | 0.89 (± 0.16) | 0.54 (± 0.13) | 0.18 (± 0.08) | 0.05 (± 0.02) | 0.09 (± 0.02) | 0.00 (± 0.02) | 0.55 (± 0.10) |

[22] After traversing the narrow Banning Pass, NMF and AMF decrease quickly in outflows, as temperature increases by ~6°C (Figure 2k). Owing to rapid volatilization of ammonium nitrate, the resulting aerosol is enriched in OMF. Rapid volatilization of ammonium nitrate has also been described for Los Angeles and Mexico City aerosols [*Huffman et al*., 2009]. The mass ratio of organics to conservative, non-volatile rBC is surprisingly constant between the Basin (131) and outflows (129), indicating that much of the secondary organic aerosol (SOA) formed in the Los Angeles Basin is relatively low in volatility, as previously reported for Los Angeles and Mexico City aerosol [*Huffman et al*., 2009]. SMF is also enhanced in outflow regions, while the ratio of sulfate to rBC does not decrease, as expected by the low volatility of sulfate species.

[23] The relative mass fractions of nonrefractory submicrometer species are compared with those reported in other megacity field experiments in Table 2. Total aerosol mass measured in the Basin during CalNex is relatively low when compared with more characteristically polluted megacities (e.g., Beijing, China; Mexico City, Mexico) and is also lower than previously reported in the Los Angeles Basin during SOAR [*Docherty et al*., 2008, 2011] and PACO [*Hersey et al*., 2011]. One reason for this discrepancy is that the month of May tends to be less photochemically active than months in the mid to late summer (July–September) and is associated with less production of SOA [*Hersey et al*., 2011]. Additionally, *Metcalf et al*. [2012] noted that Twin Otter CalNex flights were carried out during atypical May meteorology in Los Angeles, which resulted in one of the least polluted months of May in the last 25 years. The mass fractions of organics and sulfate are lower during CalNex sampling, while the fractions of nitrate and ammonium are appreciably higher than previous studies, potentially owing to less intense photochemical conditions and cooler temperatures during May 2010. The results presented here, therefore, should be considered characteristic of mild springtime conditions in Los Angeles, with similar patterns to the summertime meteorology described in section 3.1 but weaker pressure gradients and onshore winds, cooler temperatures, and less intense photochemistry.

[24] The nature and evolution of organic aerosol (OA) are of particular interest, owing to the prevalence of organic

**Table 2.** Total Mass and Relative Mass Fractions of Nonrefractory Submicron Species Measured by Aerosol Mass Spectrometry in Megacity Studies and Onboard the Twin Otter During CalNex

| Megacity Study | Total mass conc. [μg $m^{-3}$] | OMF | SMF | NMF | AMF | CMF |
|---|---|---|---|---|---|---|
| Beijing, PRC [*Sun et al*., 2009] | 71 | 0.35 | 0.25 | 0.22 | 0.16 | 0.01 |
| Mexico City, Mexico [*Aiken et al*., 2008; *DeCarlo et al*., 2008] | 31 | 0.61 | 0.15 | 0.13 | 0.09 | 0.02 |
| Pittsburgh, PA, USA [*Zhang et al*., 2005a, 2005b] | 15 | 0.3 | 0.47 | 0.06 | 0.16 | 0.01 |
| Pasadena, CA (West LA Basin) [*Hersey et al*., 2011] | 8–20 | 0.42–0.55 | 0.16–0.30 | 0.14–0.15 | 0.13–0.14 | 0–0.01 |
| Riverside, CA (East LA Basin) [*Docherty et al*., 2008; *Huffman et al*., 2009] | 19 | 0.68 | 0.13 | 0.12 | 0.06 | 0.01 |
| W. Basin [this study] | 7.7 | 0.35 | 0.13 | 0.3 | 0.18 | 0.01 |
| E. Basin [this study] | 8.2 | 0.35 | 0.06 | 0.38 | 0.17 | 0.01 |
| Outflows [this study] | 1.16 | 0.61 | 0.16 | 0.07 | 0.1 | 0 |

species in ambient particles [*Zhang et al*., 2007] and uncertainties about their formation pathways and aging. Figures 2h and 2i highlight the nature of OA in the Los Angeles Basin and outflows. The oxidation state of organics (O : C ratio; Figure 2i) is relatively constant throughout the Basin, with regional averages between 0.38 and 0.43. The mass fraction of aerosol comprised of WSOC (WMF) is similarly relatively constant throughout the Basin (0.16–0.24), as is the ratio of WMF to total organic mass (0.06–0.08). Further transport and evolution of aerosol into the outflow regions lead to significantly higher O : C ratio (0.49–0.55), WMF (0.51–0.60), and ratio of WMF to total organic mass (0.51–0.56), and *Duong et al*. [2011] found that the fraction of $PM_{2.5}$ consisting of WSOC is enhanced in outflows. Overall, aging of Los Angeles OA appears to be associated with an enhancement in the oxidiation state of organics, as has been reported in other studies of urban aerosol [*Alfarra et al*., 2004; *de Gouw et al*., 2005; *Zhang et al*., 2007; *Aiken et al*., 2008; *Kleinman et al*., 2008], as well as a significant enhancement in the mass fraction of WSOC in comparison with total organic mass. *Hersey et al*. [2011] found O : C ratios ranging from 0.44 to 0.55 at the Pasadena site relatively free from influence of primary emissions, with the highest values measured during photochemically intense conditions. *Docherty et al*. [2011] reported O : C ratios between 0.28 and 0.44 in Riverside in the eastern Basin at a site 0.5 km from a major freeway, which was influenced by reduced organics from primary vehicle emissions. The O : C ratios measured during CalNex lie between those reported by *Hersey et al*. [2011] and *Docherty et al*. [2011], owing to their distribution across areas impacted by primary emissions and those more representative of regional OA. Detailed analysis of the organic fraction of aerosol sampled onboard the Twin Otter during CalNex will follow in a subsequent manuscript.

[25] Condensation of secondary species during aging and downwind transport is further supported by observations of significant downwind enhancement of rBC coating thickness diameter of rBC particles between 90 and 270 nm, as measured by the SP2 [*Metcalf et al*., 2012]. Figure 2j indicates that the diameter of coating on rBC aerosol increases consistently from the western to eastern Basin and increases significantly as the Los Angeles plume passes through the Banning Pass and into outflows. The most dramatic increases in rBC coating thickness diameter occur in outflow regions, which are also the areas where bulk composition measurements indicate significant volatilization of semivolatile species and enhancement in OMF. These trends may be evidence of production and subsequent condensation of low-volatility SOA in outflow regions and may alternately result from dilution of the Los Angeles plume with air containing aged aerosol with thick coatings on rBC cores.

[26] In many urban areas, a smaller mode in the aerosol number distribution is dominated by OA or soot, while inorganic species and OA comprise a larger mode [*Moore et al*., 2007; *Shields et al*., 2008; *Tiitta et al*., 2010; *Sun et al*., 2009]. In Los Angeles, fine organic modes are commonly present in morning hours and during photochemically active periods in source-rich areas [*Moore et al*., 2007; *Hersey et al*., 2011] and are associated with vehicle exhaust [*Shields et al*., 2008]. Aged aerosol, such as that observed in the downwind eastern Basin, is often characterized by unimodal distributions and the presence of aged species including oligomeric compounds [*Moore et al*., 2007; *Denkenberger et al*., 2007]. Representative size-resolved non-refractory AMS composition and DMA size distribution averaged over five flights (21, 24, 25, 27, and 28 May; Figure 3) indicate that aerosol in the western Basin is characterized by a distinctly bimodal distribution, with the smaller of two modes (centered at 80–90 nm $d_{va}$) dominated by organics and the larger mode (centered at 500–600 nm $d_{va}$) dominated by nitrate in addition to containing sulfate, ammonium, and chloride. After transport to the eastern Basin, nitrate, sulfate, ammonium, and chloride still reside in the larger mode, but organics are distributed bimodally, comprising the dominant fraction of a smaller mode (60–110 nm $d_{va}$), as well as contributing a significant fraction to the larger mode (200–400 nm $d_{va}$). After transport into outflows, all species generally reside in a unimodal distribution centered at 300–400 nm $d_{va}$. One overall impact of the aging of Los Angeles aerosol appears to be that organics transition from comprising a largely separate fine mode to contributing to a single, larger mode, while inorganic species consistently reside in larger particles. Transition of an externally mixed aerosol to an internal mixture with photochemical age has been observed for bulk composition in Los Angeles [*Bhave et al*., 2001], and results here suggest that such changes in mixing state are the result of size-dependent condensation of secondary species [*Alfarra et al*., 2004].

### 3.3. Single Particle Composition

[27] AMS measurements address the overall composition of an aerosol population but are limited in their ability to determine mixing state and cannot detect refractory species. The Aerosol Time-of-Flight Mass Spectrometer (ATOFMS) measures single-particle aerosol composition for both

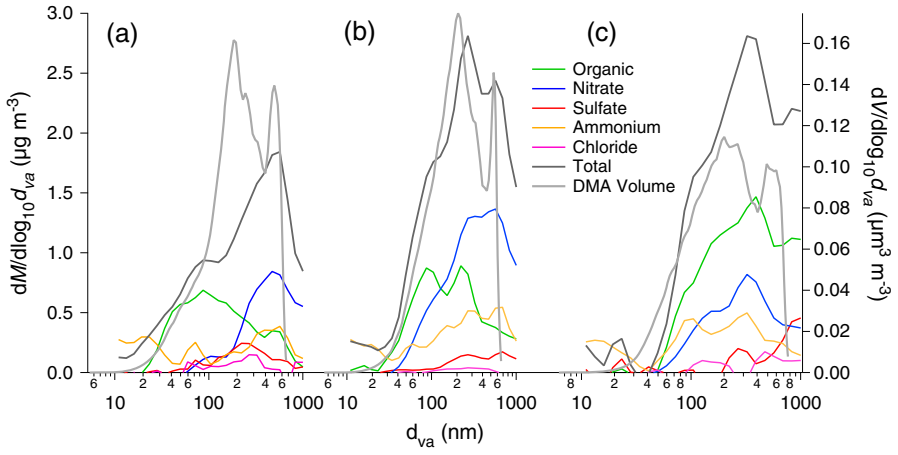


**Figure 3.** Size-resolved AMS composition and DMA volume, comparing the (a) western Basin, (b) eastern Basin, and (c) outflows, averaged over 5 flights (21, 24–25, and 27–28 May 2010). Diameter is vacuum aerodynamic ($d_{va}$).

refractory and non-refractory species and provides a direct measure of both size and mixing state. In ATOFMS analysis, single particles are classified into particle types based on dominant mass spectral peaks. ATOFMS measurements detected nine major particle types in CalNex for particles in the size range 100–300 nm $d_{va}$ (Table 3), whose representative mass spectra are represented in Figure 4. The major particle types detected were soot, soot-OC, biomass burning, highly processed, sea spray, biological, aged organic carbon, and ship emissions. Soot particles, most likely produced by vehicles [*Sodeman et al*., 2005; *Toner et al*., 2006; *Shields et al*., 2007], contained C ion subunits, $Cn^+$ ($^{12}C^+$, $^{24}C_2^+$, $^{36}C_3^+$, $^{48}C_4^+$, $^{60}C_5^+$, etc.), whereas soot-organic carbon (Soot-OC) particles were mixtures of carbon ions and smaller organic carbon ions ($^{27}C_2H_3^+$, $^{43}C_2H_3O^+$) internally mixed with nitrate ($^{62}NO_3^-$). Biomass burning particles contained a large potassium ion ($^{39/41}K^+$), potassium ion clusters ($^{104}K_2CN^+$, $^{113/115}K_2Cl^+$, $^{213/215}K_3SO_4^+$), elemental carbon, and organic carbon ions [*Silva et al*., 1999; *Pratt et al*., 2011]. Highly processed particles produced only negative ion mass spectra primarily containing sulfate ($^{97}HSO_4^-$) and/or nitrate ($^{46}NO_2^-$, $^{62}NO_3^-$) ions. Sea spray was characterized by the presence of sodium ($^{23}Na^+$), sodium clusters ($^{46}Na_2^+$, $^{62}Na_2O^+$, $^{63}Na_2OH^+$, $^{81/83}Na_2Cl^+$), and chloride ($^{35/37}Cl^-$) and internally mixed with nitrate ($^{62}NO_3^-$) [*Gaston et al*., 2011; *Gard et al*., 1998]. Biological particles contained sodium ($^{23}Na^+$), potassium ($^{39}K^+$), organic nitrogen ($^{26}CN^-$, $^{42}CNO^-$), and phosphate ($^{79}PO_4^-$) ions, and some were enriched in metals ($^{24}Mg^+$, $^{40}Ca^+$, $^{56}Fe^+$ or $^{52}Cr^+$) [*Pratt et al*., 2009b; *Russell*, 2009; *Fergenson et al*., 2003]. Aged organic carbon particles were classified based on an intense oxidized organic carbon ion ($^{43}C_2H_3O^+$) in addition to elemental and organic carbon ions [*Qin et al*., 2012]. These particles were primarily internally mixed with sulfate ($^{97}HSO_4^-$). Ship emissions were characterized by intense vanadium ($^{51}V^+$) and vanadium oxide ($^{67}VO^+$) ions which were internally mixed with sulfate ($^{97}HSO_4^-$) [*Ault et al*., 2010]. While soot was present in most particle types, characteristic soot peaks are not labeled in all mass spectra in Figure 4 because their presence is often masked by high-intensity ion peaks (e.g., that of $V^+$ in the ship emissions spectrum).

[28] Regional averages of the ATOFMS data are based on measurements of ~1000 particles in the smallest geographical regions in Figure 1 (Pasadena, Long Beach, Banning Pass) and > 4000 in larger regions (western, central, and eastern Basin). ATOFMS data are available for only one flight that sampled in outflow regions, which was heavily influenced by biomass burning emissions from a brush fire in the eastern Basin (13 May 2010) and will be considered separately. Thus, average non-biomass-burning-influenced ATOFMS data are based on five flights for which it collected data onboard the Twin Otter (6–7, 10, and 14–15 May 2010) within the Basin, with data on 13 May 2010 presented separately and including results from sampling in outflow regions.

**Table 3.** ATOFMS Particle Types, Typical Sources, and Commonly Co-emitted Species

| Type | Source | Co-emitted |
|---|---|---|
| Soot-OC | Combustion Sources, Fossil fuels | Soot, Semi-volatile organics, $SO_2$, $NO_x$, CO, $CO_2$ |
| Soot | Combustion Sources, Fossil fuels | Soot-OC, Semi-volatile organics, $SO_2$, $NO_x$, CO, $CO_2$ |
| Biomass Burning, Biomass Burning-Soot, Biomass Burning-Soot-OC | Biomass Burning | Soot, Semivolatile organics, $CH_4$, CO, $CO_2$, $N_2O$, $NH_3$, $NO_x$, $SO_2$ |
| Biological | Ocean, Soil, Spores | Dust, Sea Salt |
| Ship Emissions | Ship/bunker Fuel | Soot, Semivolatile organics, $SO_2$, $NO_x$, CO, $CO_2$ |
| Sea Spray | Ocean | Biological |
| Highly Processed Sulfate | Secondary Aerosol | Soot, Semivolatile organics, $SO_2$, $NO_x$, CO, $CO_2$, $NH_3$ |
| Highly Processed Nitrate | Secondary Aerosol | Soot, Semivolatile organics, $SO_2$, $NO_x$, CO, $CO_2$, $NH_3$ |
| Aged Organic Carbon | Secondary Aerosol | Soot, Semivolatile organics, $SO_2$, $NO_x$, CO, $CO_2$ |
| Amines, Dust, Fe, unclassified spectra | Organic Nitrogen, Arid Regions | Semivolatile organics, $CH_4$, $CO_2$, $H_2S$, $NH_3$, $NO_x$, Biological, Metals |

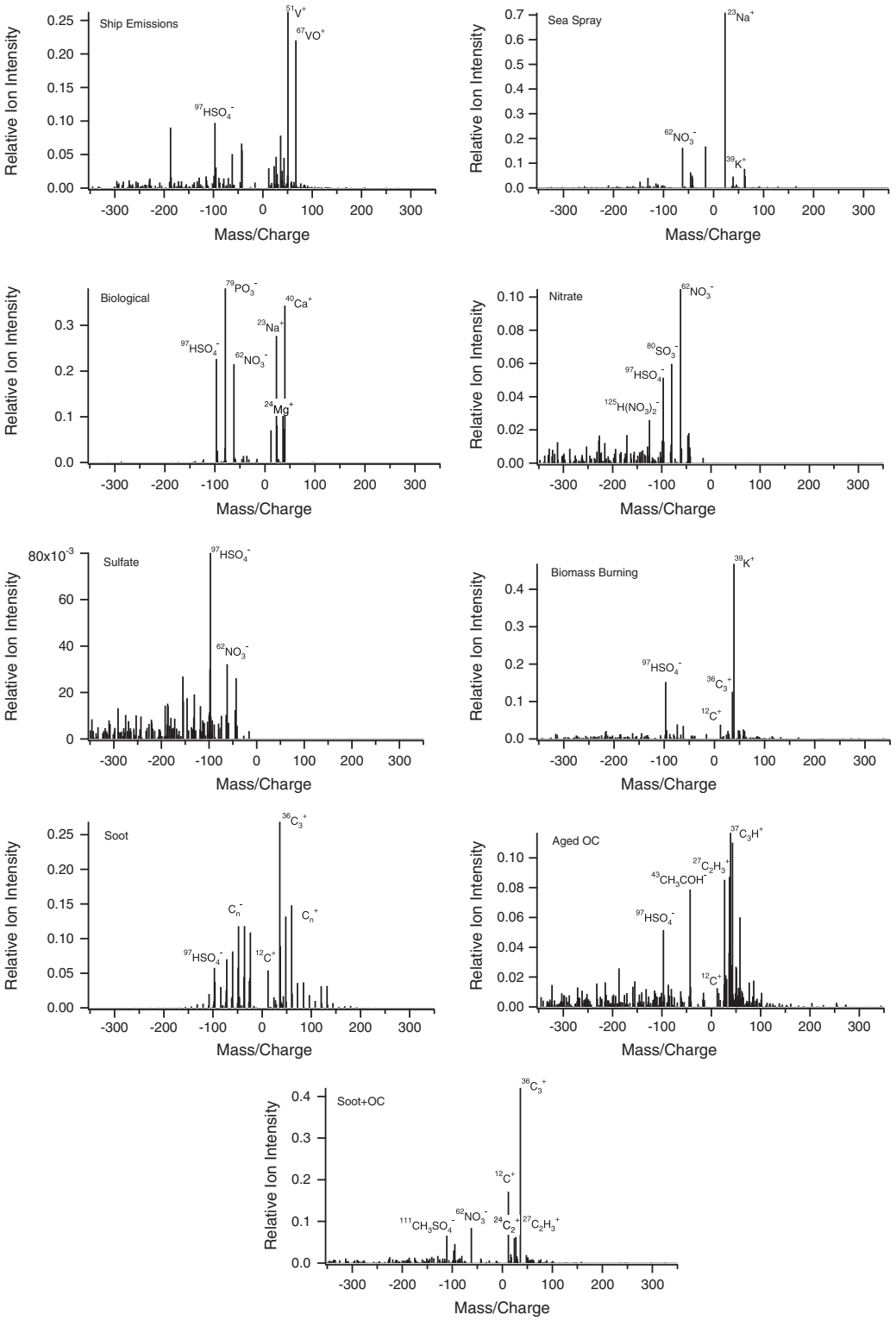


**Figure 4.** Representative positive and negative mass spectrum for each particle type identified by the ATOFMS.

[29] Characteristic particle types were identified in each region of the Basin and outflows, indicating that Los Angeles aerosol is an external mixture in the sense that not every particle has the same composition. However, each particle type identified by the ATOFMS represents an internal mixture of many different species, with nitrate and organics ubiquitous as condensed secondary material in all particle types except for pure, newly emitted soot-type particles. The areas of nitrate and organic peaks in mass spectra are enhanced in the eastern Basin relative to the western Basin, indicating that nitrate and organics become internally mixed with all particle types during downwind transport. This finding is

consistent with those from the AMS and SP2, indicating that a major characteristic of aging during downwind transport is the production and condensation of secondary organic and nitrate species.

[30] Following trends in single-particle aerosol composition from west to east in the Basin and outflows allows analysis of the effect of aging during downwind transport on both aerosol composition and mixing state in Los Angeles (Figure 5). The influence of sea spray, sulfate, and ship emissions all decrease from west to east and into outflows. The flight on 16 May 2012 was heavily influenced by sulfate particles throughout the Basin, and the small sample size in Pasadena resulted in a disproportionate enhancement in sulfate fraction in that region when compared with other regions, explaining the greater than expected influence of sulfate there. The soot + OC, Aged OC, and biomass burning particle types show little variation within the Basin, which suggests that these types of particles either have relatively uniform sources across the Basin or that they exist as background species that become well mixed throughout the Basin over hours to days. Nitrate increases in influence in eastern portions of the Basin downwind of dairies, consistent with findings from the AMS and SP2. The influence of nitrate is significantly diminished in outflows, owing to volatilization of ammonium nitrate.

[31] One would expect that soot particles become increasingly coated with secondary material during downwind transport and evolution; thus, the constant fraction of particles identified as purely soot suggests relatively uniform emissions of soot-type particles in the Basin, likely from on-road fuel combustion and widespread diesel engine use. *Pratt and Prather* [2009] heated particles to volatilize semivolatile species and found that nearly 80% of particles in the eastern Los Angeles Basin contained soot cores. To determine the fraction of particles between 100 and 300 nm $d_{va}$ possessing soot cores in the Los Angeles Basin during CalNex, single particle data were searched for soot markers in the mass spectra (*m/z* 12, 36, −36, −48, corresponding to $C^+$, $C_3^+$, $C_3^+$, and $C_4^+$, respectively). Particles with soot cores were defined as those containing soot markers at an absolute area of at least 50 on the mass spectrum [*Spencer and Prather*, 2006] and comprised 51% of particles. This result is slightly lower than reported by *Cahill et al*. [2012], who analyzed particles collected across the Basin during the 2010 CalNex study onboard the Twin Otter aircraft and determined that 60% of particles contained soot cores over the entire ATOFMS size range (100–1000 nm). Another estimate of the fraction of particles with rBC cores was obtained from the SP2 by comparing the number of particles with purely scattering signatures to the total number of particles detected by the instrument. Results indicate that the fraction of 100–300 nm particles containing rBC cores was 27 ± 15% across the Basin, with the discrepancy from ATOFMS likely due to the higher sensitivity of ATOFMS to soot (lower detection limit of ~50 nm soot cores, compared with 90 nm for the SP2) and the slightly narrower size range of SP2. We conclude that it is not possible to assign a single number to the fraction of particles with soot cores in the Los Angeles Basin but instead bracket that fraction with estimates from the SP2 and ATOFMS of 27 and 51%, respectively.

### 3.4. Subsaturated Aerosol Hygroscopicity

[32] Hygroscopicity is a function of chemical composition. Generally, inorganics are associated with a higher degree of water uptake and organics with suppressed water uptake [*Shinozuka et al*., 2009; *Quinn et al*., 2005; *Hersey et al*., 2009; *Hersey et al*., 2011]. Urban aerosol often exhibits complex hygroscopic behavior, with externally mixed particles resulting in multiple hygroscopic modes with distinct water uptake characteristics [*Cocker et al*., 2001; *Massling et al*., 2005; *Swietlicki et al*., 2008; *Massling et al*., 2009; *Meier et al*., 2009; *Tiitta et al*., 2010; *Rose et al*., 2010]. The optical sizing method employed by the DASH-SP during CalNex is limited in its ability to resolve multiple growth modes, and so subsaturated hygroscopic data reported here are for the main hygroscopic mode of particles, as is common in studies of aerosol hygroscopicity [*Wex et al*., 2010]. Subsaturated data represent particles between 175 and 225 nm dry diameter ($d_{dry}$), and hygroscopic growth was measured at RH of 74% and 92%.

[33] The $\kappa$ single-parameter measure of aerosol hygroscopicity presented by *Petters and Kreidenweis* [2007] has been widely adopted, the value of which can be derived from measurements of either subsaturated growth factor or supersaturated CCN activation. The DASH-SP measures

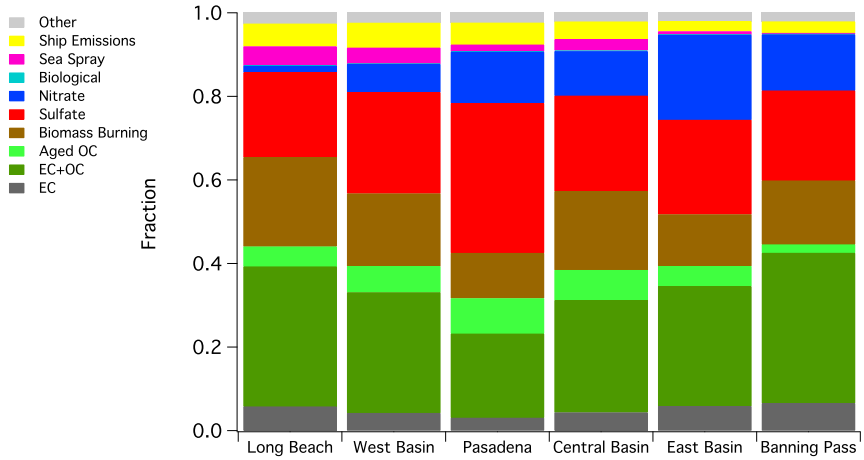


**Figure 5.** Region-averaged ATOFMS results for 100–300 nm particles, averaged over five flights (6–7, 10, and 14–15 May 2010). Numbers in parentheses are the total number of particles sampled in each region.

hygroscopic growth factor, which is the ratio of wet to dry particle diameter ($GF = d_{wet}/d_{dry}$), at a range of $d_{dry}$ and RH values. Considering that $d_{wet} = d_{dry}$ * GF, $\kappa$ may be calculated from

$$S = K \times a_w = K \frac{d_{wet}^3 - d_{dry}^3}{d_{wet}^3 - d_{dry}^3(1-\kappa)}, \quad (2)$$

where $S$ is the equilibrium water vapor saturation above the particle (i.e., RH/100), $K$ is the Kelvin term accounting for droplet curvature, $a_w$ is the activity of water, and $\kappa$ is the hygroscopicity parameter. The Kelvin term includes the droplet surface tension, to which subsaturated hygroscopicity measurements are relatively insensitive. Therefore, the surface tension of water was assumed for this study. There was no systematic difference between $\kappa$ at 74 and 92% RH, and so $\kappa$ reported here is the average of the two. Size-dependent hygroscopic behavior was not observed for particles between 175 and 225 nm during CalNex, and results here represent average hygrosopicity for particles in the DASH size range. Uncertainty in individual $\kappa$ calculations is estimated to be $\pm 0.05$, based on uncertainty in particle diameters measured by the DASH. In all regions, the standard deviation (SD) in $\kappa$ values is greater than propagated uncertainty and results are reported as $\kappa \pm$ SD.

[34] Overall, subsaturated $\kappa$ of $0.37 \pm 0.10$ in the Basin and $0.24 \pm 0.07$ in outflows during CalNex is consistent with $\kappa$ of ~0.3 reported in other megacity studies [*Shinozuka et al.*, 2009; *Chang et al.*, 2010; *Rose et al.*, 2010; *Wex et al.*, 2010]. DASH-SP averages represented in Figures 6 and 7 indicate that subsaturated water uptake of the main hygroscopic mode decreases significantly as Basin aerosols age during downwind transport. GF-derived $\kappa$ is largest in the western Basin, where a distinctly bimodal aerosol exists and AMS and SP2 indicate that the amount of organic coating material is at a minimum. In the bimodal distribution, the separate, fine mode comprises primarily organics, while inorganic species constitute the majority of aerosol mass in the DASH-SP size range. Because DASH-SP measurements represent hygroscopicity for the main hygroscopic mode for particles between 175 and 225 nm dry diameter, and because organics appear to comprise a separate mode in the aerosol, it is expected that subsaturated $\kappa$ values in the western Basin are representative of a predominantly inorganic aerosol, with a less significant contribution from condensed organic species. This characterization is consistent with an observed $\kappa$ of $\sim 0.41 \pm 0.10$ for the western Basin, assuming inorganic nitrate and sulfate species to have a representative $\kappa$ between 0.45 and 0.65 and organics to be between 0 and 0.1 [*Kreidenweis et al.*, 2008; *Massoli et al.*, 2010; *Duplissy et al.*, 2011].

[35] Hygroscopicity is suppressed in the eastern Basin relative to that in the western Basin, with an average $\kappa$ of $0.32 \pm 0.09$, corresponding to reduced SMF and CMF, condensation of significant amounts of both secondary nitrate and SOA, and a transition of much of the organic fraction to the larger mode.

[36] As noted in section 3.2, aerosols are transformed significantly during transport into outflow regions, where temperature is significantly higher and dilution is important. Volatilization results in particles that are enriched in low-volatility organic species, and continued aging causes particles

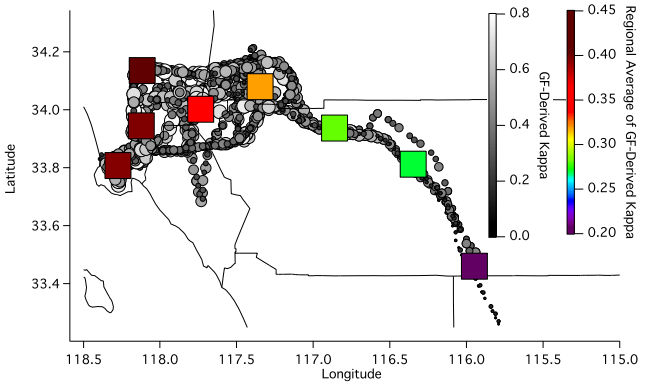


**Figure 6.** The 1 min resolution GF-derived $\kappa$ (gray circles), and regionally averaged $\kappa$ (squares) for 17 flights (4–7, 10, 12, 14–15, 18–22, 24–25, and 27–28 May 2010).

to become unimodal and thickly coated with what AMS data indicate to be predominantly organic species. Particles measured by the SP2 are not exactly in the same size range as the DASH-SP and coating thicknesses are only measured for particles with rBC cores (~27% of particles in CalNex). However, the processes by which secondary species condense onto rBC particles in the 90–270 nm size range of the SP2 will similarly tend to coat particles in the 175–225 nm size range of the DASH-SP. These general transformations by condensation of secondary coating material result in significant reduction in subsaturated hygroscopicity to $\kappa \sim 0.24 \pm 0.06$ in outflows.

[37] To further investigate the hygroscopic behavior of organics in aerosol between 175 and 225 nm $d_{dry}$, $\kappa$ values calculated from DASH-SP data were combined with representative size-resolved PTOF composition data from the AMS (Figure 3). Assuming linearly additive water uptake of each species and no interaction between aerosol constituents and representative density of 1.77 g cm$^{-3}$ for inorganics and 1.35 g cm$^{-3}$ for organics, it is possible to estimate the k for organics. If the overall hygroscopicity parameter, $\kappa$ is given by:

$$\kappa = \sum_{i=1}^{n} \kappa_i X_i \quad (3)$$

where $n$ is the number of aerosol constituents, $i$, each comprising volume fraction $\chi$ and having hygroscopicity represented by $\kappa_i$; then the organic hygroscopicity parameter, $\kappa_{org}$ can be estimated by

$$\kappa_{org} = \frac{\kappa - \sum_{i=1}^{n_{inorg}} \kappa_i X_i}{\chi_{org}} \quad (4)$$

where $n_{inorg}$ is the number of inorganic constituents, $i$, with hygroscopicity parameter $\kappa_i$ and volume fraction $\chi$, and $\chi_{org}$ is the volume fraction of organics in the aerosol. rBC is ignored in equation (4) because its volume fraction is insignificant compared with inorganic and organic species. Assuming that ammonium is associated with nitrate and sulfate according to molar ratios (i.e., 33% as ammonium nitrate and 67% as ammonium sulfate), and assuming $\kappa_i$ for ammonium nitrate, ammonium sulfate, and sea salt to be 0.67, 0.56, and 1.2, respectively, and with propagated uncertainty estimated to be $\pm 0.1$, equation (4) gives $\kappa_{org}$ of

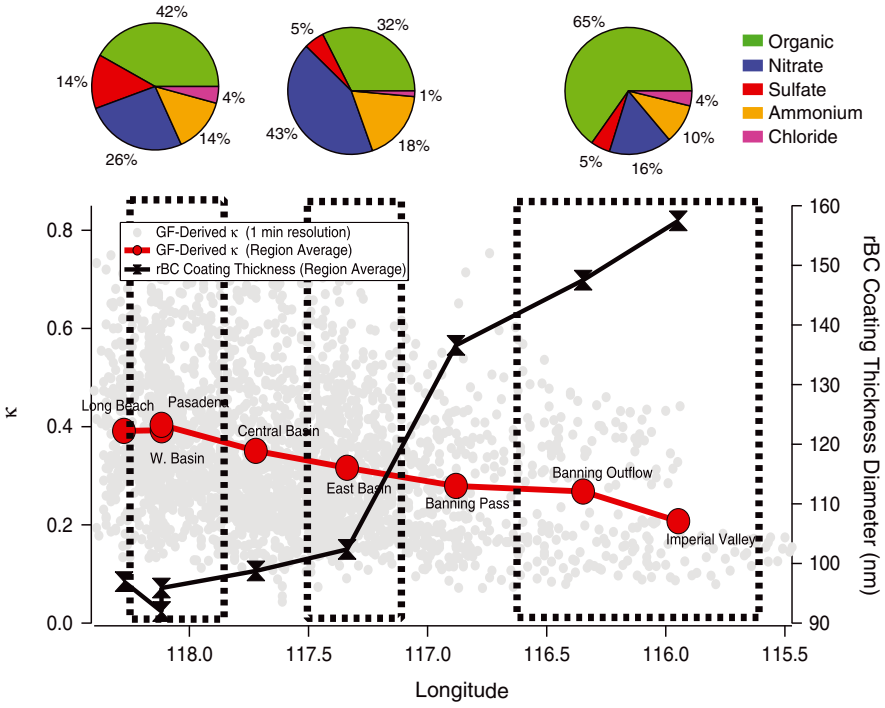


**Figure 7.** GF-derived hygroscopicity and rBC coating thickness trends with Longitude over 17 flights, from source-rich western Basin to downwind eastern Basin. Pie charts represent size-resolved AMS data for 150–250 nm particles averaged over five flights (21, 24–25, and 27–28 May 2010).

$0.1 \pm 0.1$ and $0.0 \pm 0.1$ for aerosol sampled in the western Basin and outflows, respectively. Equation (4) indicates that in the eastern Basin organics suppress water uptake below what would be expected based on the assumption of additive water uptake—a result that falls outside the range of uncertainties.

[38] Because the sheath flow is free of $NH_{3(g)}$ (section 2.6), and the DASH operates at a temperature 8°C higher than the Twin Otter inlet, the extent to which ammonium nitrate is expected to evaporate from the particles in the form of ammonia ($NH_3$) and nitric acid ($HNO_3$) is an issue that must be addressed. Here we calculate an estimate of the volatilization of ammonium nitrate (AN) in the DASH-SP by combining predictions from the thermodynamic model AIOMFAC (Aerosol Inorganic-Organic Mixtures Functional groups Activity Coefficients) [*Zuend et al.*, 2008, 2011] and the kinetic model KM-GAP (kinetic multi-layer model of gas-particle interactions in aerosols and clouds) [*Shiraiwa et al.*, 2012]. AN volatilization is modeled as a series of two distinct stages in the DASH-SP (Figure 8): (1) a drying and sizing stage, where the partial pressure of ammonia vapor ($p_{NH3}$) is initially equal to zero and the partial pressure of nitric acid vapor ($p_{HNO3}$) is equal to ambient, RH = 10%, and (2) a humidification stage, where $p_{NH3}$ and $p_{HNO3}$ are modeled as in stage 1 but RH is increased to either 74 or 92%. The residence times of particles in stages 1 and 2 are 3 and 4 s, respectively. The temperature in both stages is assumed to be 28 °C, or 8 °C higher than the characteristic aircraft inlet temperature.

[39] Based on AMS observations from CalNex, the particles are assumed to be 30% $NH_4NO_3$, 20% $(NH_4)_2SO_4$, and 50% organics in terms of dry mass fractions, with organics residing

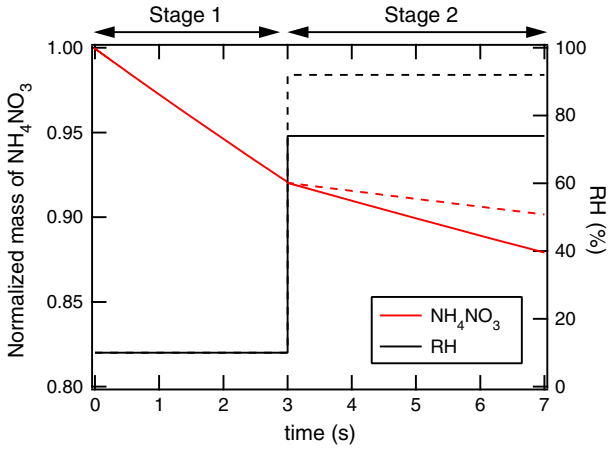


**Figure 8.** Upperbound of modeled normalized mass of ammonium nitrate (red lines) in the particle phase as a function of residence time in the DASH instrument operated at 28°C. Relative humidity (black lines) is 10% up to 3 s in stage 1 (drying and DMA) and then increased to either 74% (solid lines) or 92% (dashed lines) in stage 2 (humidification and sizing).

in a separate phase at all RH [*Song et al.*, 2012b]. Vapor-liquid equilibrium of ammonium nitrate is described by the relationship $K(T) = (a^{(m)}_{NH4+} \times a^{(m)}_{NO3-}) \; / \; (p_{NH3} \times p_{HNO3})$, with the temperature-dependent equilibrium constant $K(T)$ taken from *Seinfeld and Pandis* [2006]. The $a^{(m)}$ are molality-based activities calculated using AIOMFAC for the aqueous salt solutions at given RH. Using $D_{HNO3} = 0.120$ cm$^2$ s$^{-1}$

[*Durham and Stockburger*, 1986] and $D_{NH3} = 0.306$ cm$^2$ s$^{-1}$ [*Wu et al*., 2003] for the diffusivities in air at 28 °C, the vapor pressure of ammonia over the salt solutions is estimated to be $6.9 \times 10^{-4}$ Pa at 10% RH, $2.9 \times 10^{-4}$ Pa at 74% RH, and $1.3 \times 10^{-4}$ Pa at 92% RH. The mass loss of $NH_4NO_3$ from the particles is assumed to be stoichiometrically related to the net evaporation of ammonia. The estimated equilibrium values are used as input parameters for the mass transfer simulations with KM-GAP. The surface accommodation coefficients of $NH_3$ and $HNO_3$ are assumed to be unity. The particle aqueous phase is treated as a liquid with a bulk diffusivity of $10^{-6}$ cm$^2$ s$^{-1}$. Based on AMS results, the initial particle mass concentration and diameter are set to be 5 μg m$^{-3}$ of air and 300 nm, respectively.

[40] Figure 8 shows the results of the KM-GAP simulation. The red lines indicate the particle phase mass of $NH_4NO_3$ normalized by the initial mass. About 8% by mass of $NH_4NO_3$ is estimated to evaporate in the first stage (drying and DMA size selection) at 10% RH. Evaporation of $NH_4NO_3$ is diminished during stage 2 (humidification and optical sizing) because the equilibrium vapor pressure of $NH_3$ is inversely proportional to RH. At the outflow of stage 2, the loss of $NH_4NO_3$ is ~12% for 74% RH and ~10% for 92% RH, respectively. This thermodynamic modeling of the DASH-SP does not explicitly account for potential interactions with nafion and metal tubing in the instrument, which may potentially lead to additional nitrate loss in the instrument. However, it is expected that these losses would be less significant than those associated with removal of ammonia by filtering and temperature increases in the DASH-SP.

[41] Considering this loss of $NH_4NO_3$ in the DASH-SP, $\kappa_{org}$ was re-calculated according to equation (4), giving values of $0.2 \pm 0.1$ and $0.1 \pm 0.1$ in the western Basin and outflows, respectively. Accounting for $NH_4NO_3$ loss, this analysis indicates that organics suppress water uptake in the eastern Basin, and this result is outside the range of uncertainty. The same result is obtained whether regional averages for GF-derived $\kappa$ are based on all 17 flights or limited to the five flights for which PTOF AMS data are available.

[42] Typical values for $\kappa_{org}$ range from 0 to 0.1, depending on oxidation state [*Dusek et al*., 2010; *Wex et al*., 2010]. *Duplissy et al*. [2011] found a simple relationship between $\kappa_{org}$ and the fraction of organic signal accounted for by *m/z* 44 in the AMS spectrum ($f_{44}$) in Mexico City, resulting in enhanced $\kappa_{org}$ in oxidized organics with high $f_{44}$. Such a trend is not observed in CalNex data, with $\kappa_{org}$ appearing to be independent of organic oxidation state.

[43] While $\kappa_{org}$ for the western Basin and outflows are within the range of expected values for urban OA, organics appear to inhibit water uptake into particles in the eastern Basin. Lower-than-expected hygroscopicity may arise from a number of factors, including potential unidentified instrument artifacts. One possible explanation for apparent inhibition of water uptake in the eastern Basin involves non-ideal interactions between organic and inorganic species in the aerosol phase [*Saxena et al*., 1995; *Clegg et al*., 2001; *Zuend et al*., 2008] that have been associated with separation of amorphous organic-rich and aqueous electrolyte phases in particles [*Pankow*, 2003; *Erdakos and Pankow*, 2004; *Chang and Pankow*, 2006; *Marcolli and Krieger*, 2006]. Such liquid-liquid phase separations (LLPS) are, in fact, expected to be common in tropospheric aerosol at RH 85%, with less pronounced impact as RH approaches saturation [*Zuend et al*., 2010; *Smith et al*., 2011; *Bertram et al*., 2011; *Song et al*., 2012a; *You et al*., 2012; *Bones et al*., 2012], and may be expected to form in aerosol like that observed in the eastern Basin, thickly coated particles comprising dissolved ammonium nitrate and ammonium sulfate with an organic fraction with relatively low O : C ratio (less than ~0.4) [*Song et al*., 2012b]. If the organic-rich phase adopts a semisolid state [*Virtanen et al*., 2010; *Koop et al*., 2011; *Song et al*., 2012b; *Zuend and Seinfeld*, 2012], the rate of diffusion of water and reactive gases decreases by several orders of magnitude, effectively isolating the aqueous electrolyte core of particles from the surrounding gas phase and inhibiting establishment of thermodynamic equilibrium on the timescale of DASH-SP humidification (4 s) [*Zobrist et al*., 2011; *Shiraiwa et al*., 2011; *Tong et al*., 2011]. It is possible that the observed suppression of water uptake by organics in the eastern Basin and outflows may be the result of LLPS and kinetic limitation of water vapor accommodation, resulting in more effective suppression of hygroscopicity than predicted by models based on assumptions of internally mixed, single-phase aerosol in a liquid, low viscosity state.

### 3.5. Supersaturated (CCN) Hygroscopicity

[44] Like subsaturated hygroscopicity, CCN behavior of a population of particles of the same size is governed by chemical composition, with inorganics enhancing CCN activity and organics suppressing it. Parallel studies of subsaturated and supersaturated hygroscopicity have found the two to be correlated [e.g., *Prenni et al*., 2001], with more hygroscopic particles measured in the subsaturated regime corresponding to a higher degree of CCN activity in the supersaturated regime.

[45] By integrating the DMA number distribution from large to small sizes (since Köhler theory predicts that larger particles activate before smaller ones) and comparing to the measured droplet concentration in the CCNC, one may obtain a value for the critical diameter ($D_{crit}$), the diameter above which particles are expected to activate. The single-parameter $\kappa$ representation of Köhler theory [*Petters and Kreidenweis*, 2007] relates $D_{crit}$ to the hygroscopicity parameter $\kappa$. Once $D_{crit}$ is determined, $\kappa$ is calculated for particles corresponding to that diameter. According to Köhler theory, given an internally mixed aerosol, higher SS will correspond to CCN activation of smaller particles. Thus, the $\kappa$ values calculated at different SS give a measure of size-dependent hygroscopicity. And because hygroscopic activity is a function of particle composition, the supersaturation-resolved $D_{crit}$ and $\kappa$ measurements provide an indirect measure of size-resolved composition.

[46] Figure 9 displays regional averages of CCN-derived $\kappa$ versus $D_{crit}$ for each SS measured by the SFCA instrument, averaged over the 16 flights during which it collected data (5–7, 10, 12, 14–15, 18–22, 24–25, and 27–28 May 2010). Gray lines represent average DMA number distributions for each region. Enhanced CCN activity may result from three sources: (1) increasing SS, (2) increasing $\kappa$ (representing increased solubility), or (3) changes in mixing state (because $D_{crit}$ is calculated by integrating a DMA distribution from large to small sizes until the integrated number matches the concentration of activated particles, an external mixture with primarily insoluble material at small sizes will result in

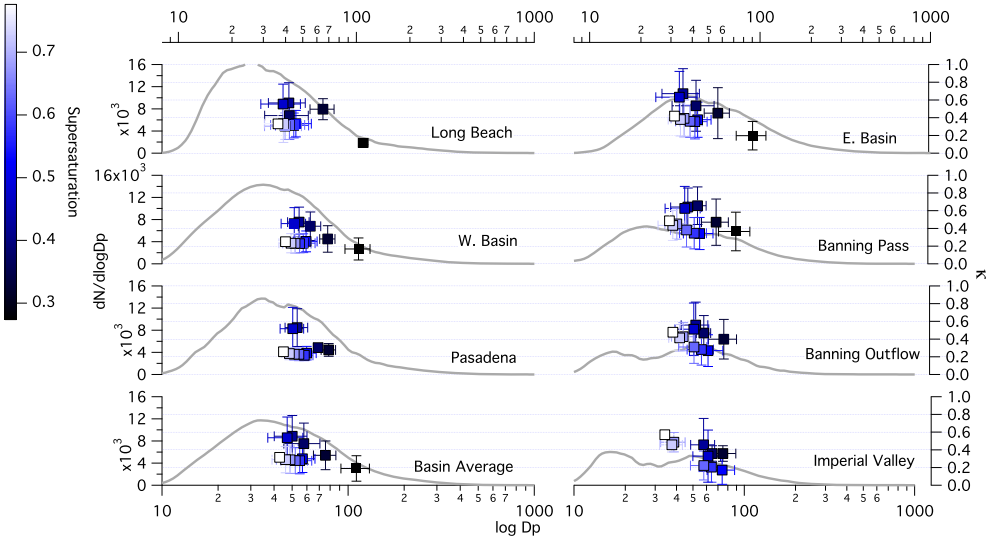


**Figure 9.** Regional averages over 16 flights (5–7, 10, 12, 14–15, 18–22, 24–25, and 27–28 May 2010) of aerosol hygroscopicity, $\kappa$, calculated from mean size distributions (gray line) and measured CCN concentrations, plotted against critical diameter ($D_{crit}$), for supersaturation (SS) ranging from 0.275–0.775%.

increased $D_{crit}$, and thereby smaller $\kappa$). In each region, $D_{crit}$ decreases with increased supersaturation. Because CCN activity is a function of SS, hygroscopicity, and mixing state, the extent to which $D_{crit}$ decreases with increased SS indicates whether an aerosol is impacted by insoluble material or an external mixture. Within the Basin, $D_{crit}$ decreases significantly as SS increases from 0.275 to 0.375%, and the most hygroscopic particles ($\kappa \sim 0.4$–$0.6$) correspond to 60–70 nm particles measured at $0.425\% < SS < 0.475\%$. Further increases in supersaturation do not result in significant decreases in $D_{crit}$, suggesting an externally mixed aerosol with particles smaller than 60 nm comprising nonhygroscopic material. This conclusion is consistent with previous findings in Los Angeles and Beijing that small organics behave as nonactivating or only slightly hygroscopic in CCN activity [*Cubison et al.*, 2005; *Gunthe et al.*, 2011]. Indeed, overall $\kappa$ calculated for particles < 60 nm at SS > 0.475% is low in the Basin (0.2–0.3). These results are consistent with the observation of a small mode in the aerosol comprised predominantly of organics condensed onto soot particles (sections 3.2 and 3.3). Particles that activate at SS < 0.375% in the LA Basin are significantly larger (~ 100 nm), corresponding roughly to the DASH-SP size range. CCN-derived $\kappa$ of these particles is 0.2–0.4, comparing favorably with GF-derived $\kappa$ (0.3–0.4). Size-resolved AMS and ATOFMS data for 100–300 nm particles indicate that these particles comprise several distinct types, including pure soot and organic-coated soot at the smallest sizes.

[47] In the Banning Pass and outflow regions, $D_{crit}$ similarly decreases with increased SS from 0.275 to 0.375%. Further increases in SS from 0.375 to 0.625% do not correspond to significant decreases in $D_{crit}$, suggesting that the majority of particles in this size range (50–70 nm) are relatively non-hygroscopic. This observation is consistent with that from PToF AMS data that a fine mode exists, comprised almost entirely of organics and with ATOFMS evidence of an external mixture dominated by biomass burning particles in the outflow regions. Further increases in SS (> 0.625%) in outflows correspond to significant decreases in $D_{crit}$ (approaching 30 nm) and increases in $\kappa$ (approaching 0.7), suggesting an external mixture with the smallest particles containing hygroscopic inorganic material.

[48] Figures 10 and 11 display west-east trends in CCN-derived hygroscopicity for particles that activate at 0.325% and 0.725% SS (~ 70–120 and 30–60 nm $D_{crit}$, respectively), as well as regionally averaged size-resolved composition and coating thickness. As noted in section 3.4, the size range measured by the SP2 is 90–270 nm rBC cores. While this size range does not directly compare with the CCN diameters measured at 0.325 and 0.725% SS, the processes that result in condensation of secondary coatings on these rBC particles will also result in significant coatings on particles in the CCN size range. Thus, comparison of coating thickness on rBC particles in the SP2 size range with CCN particles of 30–120 nm can provide a valuable framework for understanding the types of transitions to which these fine particles are subject during downwind transport. At 0.325% SS, there is a clear trend of increasing hygroscopicity from west to east in the Basin, corresponding to an increase in coating thickness diameter and the fraction of nitrate and ammonium on particles. Further transport and evolution into outflows correspond to decreased prevalence of nitrate, enhanced coating thickness, and suppressed CCN-derived hygroscopicity. At 0.725% SS, particles similarly increase in hygroscopicity during downwind transport from the western to eastern Basin, corresponding to an increase in coating thickness and the fraction of nitrate in small particles. Volatilization of semivolatile species, leaving low-volatility organics and sulfate, translate to relatively constant hygroscopicity in outflows. These supersaturated hygroscopicity results suggest that the nitrate and organic coatings added to particles during downwind transport and evolution serve to enhance CCN activity, despite tending to suppress subsaturated hygroscopicity (section 3.4). Overall, CCN-derived $\kappa$ averaged $0.35 \pm 0.12$ in the Basin and $0.38 \pm 0.11$ in Outflows – values that are 15–25% higher than previous studies that have

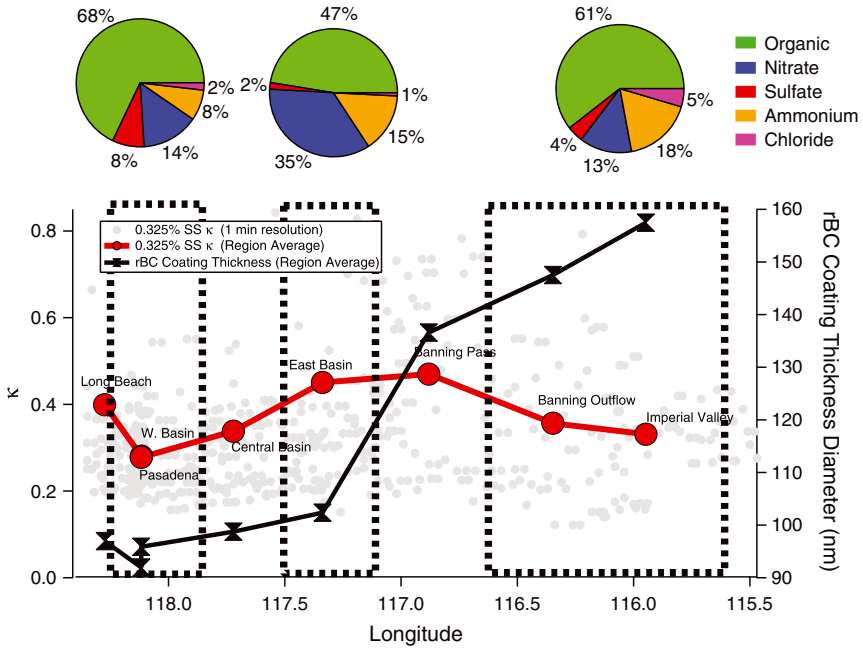


**Figure 10.** Average over 16 flights of CCN-derived κ (0.325% SS) and rBC coating thickness trends with longitude from source-rich western to downwind eastern areas of the LA Basin. Pie charts represent size-resolved AMS data for 70–120 nm particles averaged over five flights (21, 24–25, and 27–28 May 2010).

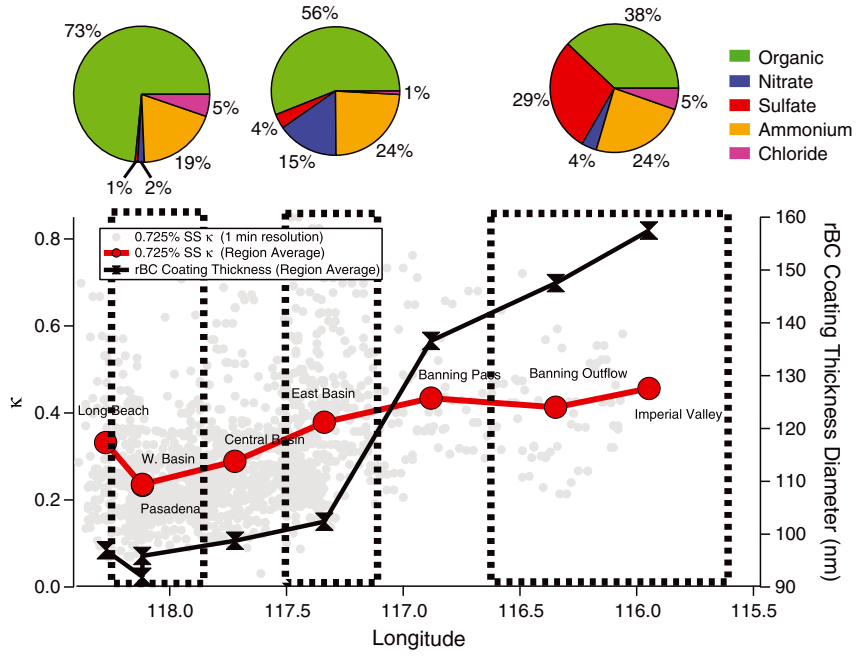


**Figure 11.** Average over 16 flights of CCN-derived $\kappa$ (0.725% SS) trends with longitude from source-rich western to downwind eastern areas of the LA Basin. Pie charts represent size-resolved AMS data for 30–60 nm particles averaged over five flights (21, 24–25, and 27–28 May 2010).

suggested urban aerosol hygroscopicity may be estimated by $\kappa \sim 0.3$ [*Shinozuka et al.*, 2009; *Chang et al.*, 2010; *Rose et al.*, 2010; *Wex et al.*, 2010].

[49] Hygroscopicity of the organic fraction ($\kappa_{org}$) was estimated for CCN particles by employing equation (4) and the method described in section 3.4 and utilizing size-resolved PTOF AMS data for particles between ~30–60 nm (0.725% SS) and ~70–120 nm (0.325% SS). Results indicate that $\kappa_{org}$ is independent of region for CCN-derived hygroscopicity, remaining a constant $0.1 \pm 0.1$ throughout the western and eastern Basin and outflows. These values are comparable to subsaturated GF-derived $\kappa_{org}$ except in the eastern Basin,

where organics appear to suppress water uptake in the subsaturated regime but contribute somewhat to supersaturated hygroscopicity.

### 3.6. Influence of Biomass Burning from a Localized Brush Fire

[50] On 13 May 2010, a brush fire was sparked at ~13:30 LT in Riverside County in the eastern Los Angeles Basin, burning 500 acres before being contained later that evening. Twin Otter takeoff time on 13 May was 11:06 and landing was at 14:51 P.M. The Twin Otter sampled in biomass-burning-influenced air for nearly 90 min near the end of the flight. The Twin Otter sampled within both the Basin and outflow regions and was positioned to sample both the immediate vicinity of the brush fire and the downwind, aged biomass burning aerosol. On 13 May ATOFMS data indicate that the biomass burning particle type number was enhanced by ~500 and 1100% in the west and east Basin, respectively, and constitute ~41 and 60% of particles in the west and east Basin, respectively, as compared with ~7 and 5% during non-biomass-burning-influenced flights. In outflow regions on 13 May biomass burning particles represented 58% of particles between 100 and 300 nm $d_{va}$ (Figures 12a and 12b). These enhancements in biomass burning particles are associated with significant suppression of subsaturated hygroscopicity, but an enhancement in CCN concentration, CCN activation ratio (AR), and CCN-derived hygroscopicity (Table 4). Biomass burning particles have been identified as important sources of CCN [*Hennigan et al.*, 2012]. *Petters et al.* [2009] determined that biomass burning particles tend to be CCN active at the point of emissions, but subsaturated $\kappa$ of particles tend to be suppressed under the influence of biomass burning [*Petters et al.*, 2009; *Rose et al.*, 2010; *Dusek et al.*, 2011]. *Dusek et al.* [2011] found that biomass burning influence can result in surface-active organics and phase separation of species in aerosols. This leads to discrepancies between subsaturated and CCN-derived hygroscopicity (with subsaturated $\kappa$ suppressed relative to CCN $\kappa$). Under the influence of biomass burning, CCN concentrations and activation ratios tend to be enhanced by the production of new CCN-active particles, while if surface-active organic species induce phase separation, hygroscopicity is suppressed at subsaturated RH.

### 3.7. Comparison of GF- and CCN-Derived Hygroscopicity

[51] One would expect subsaturated and supersaturated hygroscopicity to be correlated, with higher subsaturated $\kappa$ tending to correspond to lower critical diameters for cloud droplet activation. Aerosols in the Los Angeles Basin are compositionally complex, with significant evolution in bulk and size-resolved composition and mixing state between source-rich and downwind areas. This evolution in composition results in complex hygroscopic behavior and discrepancies between GF- and CCN-derived hygroscopicity.

[52] In the western and Central LA Basin, subsaturated and supersaturated hygroscopicity measurements display relatively good agreement when hygroscopicity is calculated for similarly sized particles (GF-derived $\kappa$ 0.3–0.4 for $D_{p,dry}$ 175–225 nm, versus 0.2–0.4 for CCN measurements at 0.275–0.375% SS and corresponding to particles ~100 nm in diameter). In the nitrate-rich eastern Basin, subsaturated

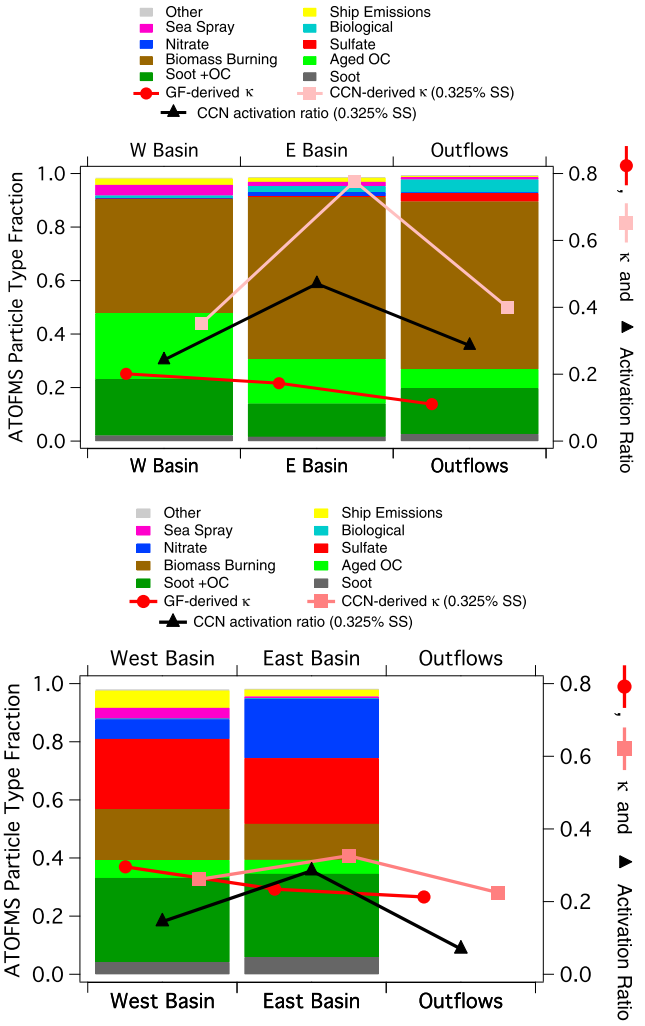


**Figure 12.** Comparison of ATOFMS particle type fraction, GF-derived $\kappa$, CCN-derived $\kappa$ (0.325% SS), and activation ratio for (a) 13 May 2010 and (b) five non-biomass-burning-influenced flights (6–7, 10, and 14–15 May 2010).

and supersaturated hygroscopicity measurements disagree. Disagreements between subsaturated and supersaturated estimates of the hygroscopicity parameter $\kappa$ have been noted in a number of studies and have been attributed to factors such as differences in size-resolved composition and instrument operating conditions, adsorption of gases in sampling lines, as well as nonideal effects of solutes on water activity and surface tension [*Good et al.*, 2010; *Irwin et al.*, 2010, 2011; *Sareen et al.*, 2012]. In CalNex there is some evidence of size-dependent differences in composition between particles in the CCN and DASH size ranges, despite their residing in the same mode of the DMA distribution (Figure 3). Also, as discussed in section 3.2, evolution in aerosol from the western to eastern Basin is associated with a transition of the organic-soot fraction from a small mode in the aerosol to a larger, unimodal fraction. *Pratt and Prather* [2009] observed similar evidence of internally mixed aerosols in aged plumes in the eastern Los Angeles Basin, owing to condensation of secondary species onto primary particulates. CCN measurements of hygroscopicity may be biased low in the case where aerosol exists as an external mixture with the smallest particles

**Table 4.** Influence of Biomass Burning on Subsaturated Hygroscopicity, CCN Concentration, and Activation Ratio (AR) and CCN-Derived $\kappa$ at 0.325% SS

| | | Non-BB-Influenced | 13 May 2010 | % Change |
|---|---|---|---|---|
| W. Basin | GF $\kappa$ | 0.39 | 0.20 | −0.49% |
| | CCN $cm^{-3}$ | 1569 | 1714 | + 9% |
| | 0.325% SS AR | 0.14 | 0.24 | + 67% |
| | 0.325% SS $\kappa$ | 0.26 | 0.35 | + 35% |
| E. Basin | GF $\kappa$ | 0.32 | 0.18 | −0.44% |
| | CCN $cm^{-3}$ | 2116 | 3064 | + 45% |
| | 0.325% SS AR | 0.29 | 0.47 | + 65% |
| | 0.325% SS $\kappa$ | 0.33 | 0.78 | + 138% |
| Outflows | GF $\kappa$ | 0.24 | 0.13 | −0.46% |
| | CCN $cm^{-3}$ | 274 | 1189 | + 335% |
| | 0.325% SS AR | 0.07 | 0.29 | + 310% |
| | 0.325% SS $\kappa$ | 0.23 | 0.40 | + 78% |

composed primarily of insoluble organic material. The transition from externally mixed to internally mixed aerosol from west to east in the Basin and elimination of this small insoluble mode by growth and condensation of secondary material would tend to enhance CCN activity, but the condensation of organics on a unimodal aerosol comprising the main hygroscopic mode would tend to result in suppressed subsaturated hygroscopicity as measured by the DASH-SP, thus leading to a disagreement between the two measurements.

[53] The discrepancy between subsaturated hygroscopicity and CCN activity in areas of the eastern Basin and the disagreement between subsaturated and supersaturated RH estimates of $\kappa_{org}$ suggests that the delay of water uptake by organics is more pronounced at RH < 100%. As discussed in section 3.4, LLPS and the presence of an amorphous organic layer is one possible explanation for the observed suppression of subsaturated hygroscopicity evidenced by estimates of $\kappa_{org}$. *Dusek et al*. [2011] found similar disagreement between subsaturated hygroscopicity and CCN activity under the influence of LLPS, but general agreement between the two when aerosols appeared to be comprised of a single liquid phase. While results here are not conclusive evidence of LLPS, it is possible that condensation of secondary organics onto particles during aging in the Los Angeles Basin results in separate organic coating layers that form a barrier to water vapor accommodation. However, this effect is primarily observed in subsaturated measurements of hygroscopicity with short humidification residence times, as opposed to supersaturated measurements of CCN activity.

## 4. Conclusions

[54] Aerosols age as they are transported from source-rich sites in the western Los Angeles Basin to downwind receptor sites in the eastern Basin and desert outflow regions. Within the Basin, this aging is associated with increased rBC coating thickness and increased mass of ammonium, nitrate, and organics, owing to the production and condensation of secondary species. In the relatively source-rich western areas of the Basin, the aerosol distribution comprises a small mode of predominantly organic species mixed with soot and a larger accumulation mode consisting primarily of inorganics coated on soot-organic cores. Condensation of secondary species results in a unimodal aerosol at downwind receptor sites in the eastern Basin and outflows. With increasing age in the Basin, aerosols become internally mixed, with secondary nitrate and organics detected on most particles. Transport into desert outflow regions is associated with dilution and volatilization of semivolatile species, and the resulting aerosol consists of predominantly low-volatility, oxidized, water-soluble organics and sulfate. It is not possible on the basis of the available measurements to infer a single number for the overall fraction of particles with soot cores in Los Angeles; results from the SP2 and ATOFMS indicate a range of 27–51%.

[55] Transformations in aerosol composition during downwind transport and aging have different effects on hygroscopicity at subsaturated and supersaturated RH. Subsaturated and supersaturated hygroscopicity measurements tend to agree in the western Basin, but at subsaturated RH, $\kappa$ is suppressed significantly in the eastern Basin and outflows as secondary nitrate and organics condense onto particles in the 175–250 nm size range. Calculations of $\kappa_{org}$ suggest that organics inhibit water uptake in the eastern Basin and are nonhygroscopic in outflows. Subsaturated water uptake appears to be inhibited by organics in the eastern Basin, and one possible explanation for this behavior is the formation of separate, organic layers that inhibit water uptake on humidification timescales similar to those in the DASH-SP. Supersaturated hygroscopicity is highest for particles on the order of 60–70 nm in the Basin, with smaller particles (identified organics mixed with soot) appearing to be nonhygroscopic. CCN-derived hygroscopicity is enhanced when rBC coating thickness increases, and CCN-derived $\kappa_{org}$ is spatially invariant at $0.1 \pm 0.1$, suggesting that the potential inhibition of water uptake by layers of secondary organics primarily affects subsaturated water uptake. Other sources of discrepancy between subsaturated and supersaturated hygroscopicity measurements include size-dependent variation in composition within the small aerosol mode, as well as the apparent conversion of externally mixed aerosol to one that is internally mixed, which tends to enhance CCN activity but result in suppressed subsaturated water uptake of the main hygroscopic mode.

[56] Finally, a small brush fire in the eastern Basin on 13 May 2010 quickly (on the order of 1–2 h) and significantly enhanced the concentration of the biomass burning particle type throughout much of the Los Angeles area. Enhancements in biomass burning aerosols resulted in significant suppression of water uptake at subsaturated RH, but enhanced CCN activity, consistent with previous findings that biomass burning particles are relatively nonhygroscopic but yet are CCN active.

[57] **Acknowledgment.** This work was supported by NOAA grant NA09OAR4310128 and CARB agreement #09-333.

## References

Aiken, A. C., et al. (2008), O/C and OM/OC ratios of primary, secondary, and ambient organic aerosols with high-resolution time-of-flight aerosol mass spectrometry, *Environ. Sci. Technol.*, *42*, 4478–4485, doi:10.1021/es703009q.

Alfarra, M. R., et al. (2004), Characterization of urban and rural organic particulate in the lower Fraser valley using two Aerodyne aerosol mass spectrometers, *Atmos. Environ.*, *38*, 5745–5758, doi:10.1016/j.atmosenv.2004.01.054.

AQMD, (2012), Historic ozone air quality trends, available at: http://www.aqmd.gov/smog/o3trend.html.

Ault, A. P., C. J. Gaston, Y. Wang, G. Dominguez, M. H. Thiemens, and K. A. Prather (2010), Characterization of the single particle mixing state of

individual ship plume events measured at the port of Los Angeles, *Environ. Sci. Technol.*, *44*, 1954–1961, doi:10.1021/es902985h.

Baumgardner, D., G. L. Kok, and G. Raga (2004), Warming of the Arctic lower stratosphere by light absorbing particles, *Geophys. Res. Lett.*, *31*, L06117, doi:10.1029/2003GL018883

Baumgardner, D., et al. (2012), Soot reference materials for instrument calibration and intercomparisons: A workshop summary with recommendations. *Atmos. Meas. Tech.*, *5*, 1869–1887, doi:10.5194/amt-5-1869-2012.

Bertram, A. K., S. T. Martin, S. J. Hanna, M. L. Smith, A. Bodsworth, Q. Chen, M. Kuwata, A. Liu, Y. You, and S. R. Zorn (2011), Predicting the relative humidities of liquid-liquid phase separation, efflorescence, and deliquescence of mixed particles of ammonium sulfate, organic material, and water using the organic-to-sulfate mass ratio of the particle and the oxygen-to-carbon elemental ratio of the organic component, *Atmos. Chem. Phys. Discuss.*, *11*, 17759–17788, doi:10.5194/acpd-11-17759-2011.

Bhave, P. V., D. P. Fergenson, K. A. Prather, and G. R. Cass (2001), Source apportionment of fine particulate matter by clustering single-particle data: Tests of receptor model accuracy, *Environ. Sci. Technol.*, *35*, 2060–2072.

Blumenthal, D., W. White, and T. Smith (1978), Anatomy of a Los Angeles smog episode: Pollutant transport in the daytime sea breeze regime, *Atmos. Environ.*, *12*, 893–907.

Bones, D. L., J. P. Reid, D. M. Lienhard, and U. K. Krieger (2012), Comparing the mechanism of water condensation and evaporation in glassy aerosol, *Proc. Natl. Acad. Sci. U. S. A.*, *109*, doi:10.1073/pnas.1200691109.

Cahill, J. F., K. Suski, J. H. Seinfeld, R. A. Zaveri, and K. A. Prather (2012), The mixing state of carbonaceous aerosol particles in Northern and Southern California measured during CARES and CalNex 2010, *Atmos. Chem. Phys. Discuss.*, *12*, 18419–18457, doi:10.5194/acpd-12-18419-2012.

Chang, E. I., and J. F. Pankow (2006), Prediction of activity coefficients in liquid aerosol particles containing organic compounds, dissolved inorganic salts, and water—Part 2: Consideration of phase separation effects by an X-UNIFAC model, *Atmos. Environ.*, *40*, 6422–6436, doi:10.1016/j.atmosenv.2006.04.031.

Chang, R. Y., J. G. Slowik, N. C. Shantz, A. Vlasenko, J. Liggio, S. J. Sjostedt, W. R. Leaitch, and J. P. D. Abbatt (2010), The hygro-scopicity parameter ($\kappa$) of ambient organic aerosol at a field site subject to biogenic and anthropogenic influences: Relationship to degree of aerosol oxidation, *Atmos. Chem. Phys.*, *10*, 5047–5064, doi:10.5194/acp-10-5047-2010.

Chow, J., E. Fujita, J. Watson, Z. Lu, D. Lawson, and L. Asbaugh (1994), Evaluation of filter-based aerosol measurements during the 1987 Southern California Air-Quality Study, *Environ. Monit. Assess.*, *30*, 49–80, doi:10.1007/BF00546199.

Clegg, S. L., J. H. Seinfeld, and P. Brimblecombe (2001), Thermodynamic modelling of aqueous aerosols containing electrolytes and dissolved organic compounds, *J. Aerosol. Sci.*, *32*(713–738), 2001.

Cocker, D. R., N. E. Whitlock, R. C. Flagan, and J. H. Seinfeld (2001), Hygroscopic properties of Pasadena, California aerosol, *Aerosol Sci. Technol.*, *35*, 637–647.

Collins, D. R., R. C. Flagan, and J. H. Seinfeld (2002), Improved inversion of scanning DMA data, *Aeorosol. Sci. Tech.*, *36*(1), 1–9, doi:10.1080/02786820275333903 2.

Croes, B., and E. Fujita (2003), Overview of the 1997 Southern California Ozone Study (SCOS97-NARSTO), *Atmos. Environ.*, *37*, S3–S26, doi:10.1016/S1352-2310(03)003790.

Cubison, M. J., B. Ervens, G. Feingold, K. S. Docherty, I. M. Ulbrich, L. Shields, K. Prather, S. Hering, and J. L. Jimenez (2008), The influence of chemical composition and mixing state of Los Angeles urban aerosol on CCN number and cloud properties, *Atmos. Chem. Phys.*, *8*(18), 5649–5667, doi:10.5194/acp-8-5649-2008.

DeCarlo, P. F., et al. (2008), Fast airborne aerosol size and chemistry measurements above Mexico City and Central Mexico during the MILAGRO campaign, *Atmos. Chem. Phys.*, *8*, 4027–4048, doi:10.5194/acp-8-4027-2008.

de Gouw, J. A., et al. (2005), Budget of organic carbon in a polluted atmosphere, Results from the New England Air Quality Study in 2002, *J. Geophys. Res. Atmos.*, *110*, D16305, doi:16310.11029/12004JD00562.

Denkenberger, K. A., R. C. Moffet, J. C. Holecek, T. P. Rebotier, and K. A. Prather (2007), Real-time, single-particle measurements of oligomers in aged ambient aerosol particles, *Environ. Sci. Technol.*, *41*, 5439–5446, doi:10.1021/es070329l.

Docherty, K. S., et al. (2008), Apportionment of primary and secondary organic aerosols in Southern California during the 2005 Study of Organic Aerosols in Riverside (SOAR-1), *Environ. Sci. Technol.*, *42*, 7655–7662, doi:10.1021/es8008166.

Docherty, K. S., et al. (2011), The 2005 Study of Organic Aerosols at Riverside (SOAR-1): Instrumental intercomparisons and fine particle composition, *Atmos. Chem. Phys.*, *11*, 12387–12420, doi:10.5194/acp-11-12387-2011.

Drewnick, F., et al. (2005), A new time-of-flight aerosol mass spectrometer (TOF-AMS)—Instrument description and first field deployment, *Aerosol Sci. Technol.*, *39*(7), 637–658, doi:10.1080/02786820500182040.

Duong, H. T., A. Sorooshian, J. S. Craven, S. P. Hersey, A. R. Metcalf, X. Zhang, R. J. Weber, H. Jonsson, R. C. Flagan, and J. H. Seinfeld (2011), Water-soluble organic aerosol in the Los Angeles Basin and outflow regions: Airborne and ground measurements during the 2010 CalNex field campaign, *J. Geophys. Res.*, *116*, D00V04, doi:10.1029/2011JD016674.

Duplissy, J., et al. (2011), Relating hygroscopicity and composition of organic aerosol particulate matter, *Atmos. Chem. Phys.*, *11*, 1155–1165, doi:10.5194/acp-11-1155-2011.

Durham, J. L., and L. Stockburger (1986), Nitric acid-air diffusion coefficient: Experimental determination, *Atmos. Environ.*, *20*(3), 559–563.

Dusek, U., G. P. Frank, J. Curtius, F. Drewnick, J. Schneider, A. Kurten, D. Rose, M. O. Andreae, S. Borrmann, and U. Poschl (2010), Enhanced organic mass fraction and decreased hygroscopicity of cloud condensation nuclei (CCN) during new particle formation events, *Geophys. Res. Lett.*, *37*, L03804, doi:10.1029/2009GL040930.

Dusek, U., G. P. Frank, A. Massling, K. Zeromskiene, Y. Iinuma, O. Schmid, G. Helas, T. Henning, A. Wiedensohler, and M. O. Andreae (2011), Water uptake by biomass burning aerosol at sub- and supersaturated conditions: Closure studies and implications for the role of organics, *Atmos. Chem. Phys.*, *11*, 9519–9532, doi:10.5194/acp-11-9519-2011.

Eatough, D. J., B. D. Grover, W. R. Woolwine, N. L. Eatough, R. Long, and R. Farber (2008), Source apportionment of 1 h semicontinuous data during the 2005 Study of Organic Aerosols in Riverside (SOAR) using positive matrix factorization, *Atmos. Environ.*, *42*, 2706–2719, doi:10.1016/j.atmosenv.2007.07.038.

Eldering, A., G. Cass, and K. Moon (1994), An air monitoring network using continuous particle-size distribution monitors—Connecting pollutant properties to visibility via mie scattering calculations, *Atmos. Environ.*, *28*, 2733–2749, doi:10.1016/13522310(94)90445-6.

Erdakos, G. B., and J. F. Pankow (2004), Gas/particle partitioning of neutral and ionizing compounds to single- and multi-phase aerosol particles. 2. Phase separation in liquid particulate matter containing both polar and low-polarity organic compounds, *Atmos. Environ.*, *38*, 1005–1013, doi:10.1016/j.atmosenv.2003.10.038.

Fergenson, D. P., et al. (2003), Reagentless detection and classification of individual bioaerosol particles in seconds, *Anal. Chem.*, *76*, 373–378, doi:10.1021/ac034467e.

Gard, E. E., et al. (1998), Direct observation of heterogeneous chemistry in the atmosphere, *Science*, *279*, 1184–1187.

Gaston, C. J., et al. (2011), Unique ocean-derived particles serve as a proxy for changes in ocean chemistry, *J. Geophys. Res. Atmos.*, *116*, doi:10.1029/2010JD015289.

Good, N., D. O. Topping, J. D. Allan, M. Flynn, E. Fuentes, M. Irwin, P. I. Williams, H. Coe, and G. McFiggans (2010), Consistency between parameterizations of aerosol hygroscopicity and CCN activity during the RHaMBLe discovery cruise, *Atmos. Chem. Phys.*, *10*, 3189–3203, doi:10.5194/acp-10-3189-2010.

Gunthe, S. S., et al. (2011), Cloud condensation nuclei (CCN) from fresh and aged air pollution in the megacity region of Beijing, *Atmos. Chem. Phys.*, *11*, 11023–11039, doi:10.5194/acp-11-11023-2011.

Heck, R. M. (1999), Catalytic abatement of nitrogen oxides—Stationary applications, *Catal. Today*, *53*, 519–523.

Hennigan, C. J., D. M. Westervelt, I. Riipinen, G. L. Engelgart, T. Lee, J. L. Collett, S. N. Pandis, P. J. Adams, and A. L. Robinson (2012), New particle formation and growth in biomass burning plumes: An important source of cloud condensation nuclei, *Geophys. Res. Lett.*, *39*, doi:10.1029/2012GL050930.

Hersey, S. P., A. Sorooshian, S. M. Murphy, R. C. Flagan, and J. H. Seinfeld (2009), Aerosol hygroscopicity in the marine atmosphere: A closure study using high-time-resolution, multiple-RH DASH-SP and size-resolved C-ToF-AMS data, *Atmos. Chem. Phys.*, *9*, 2543–2554.

Hersey, S. P., J. S. Craven, K. A. Schilling, A. R. Metcalf, A. Sorooshian, M. N. Chan, R. C. Flagan, and J. H. Seinfeld (2011), The Pasadena aerosol characterization observatory (PACO): Chemical and physical analysis of the western Los Angeles Basin aerosol, *Atmos. Chem. Phys.*, *11*, 7417–7443, doi:10.5194/acp-11-7417-2011.

Huffman, J. A., et al. (2009), Chemically-resolved aerosol volatility measurements from two megacity field studies, *Atmos. Chem. Phys.*, *9*, 7161–7182, doi:10.5194/acp-9-7161-2009.

Hughes, L., J. Allen, L. Salmon, P. Mayo, R. Johnson, and G. Cass (2002), Evolution of nitrogen species air pollutants along trajectories crossing the Los Angeles area, *Environ. Sci. Technol.*, *36*, 3928–3935, doi:10.1021/es0110630.

Irwin, M., Good, N., J. Crosier, T. W. Choularton, and G. McFiggans (2010), Reconciliation of measurements of hygroscopic growth and critical supersaturation of aerosol particles in central Germany, *Atmos. Chem. Phys.*, *10*, 11737–11752, doi:acp-10-11737-2010.

Irwin, M., N. Robinson, J. D. Allan, H. Coe, and G. McFiggans (2011), Size-resolved aerosol water uptake and cloud condensation nuclei measurements as measured above a Southeast Asian rainforest

during OP3, *Atmos. Chem. Phys*, *11*, 11157–11174, doi:acp-11-11157-2011.

Jayne, J. T., D. C. Leard, X. Zhang, P. Davidovits, K. A. Smith, C. E. Kolb, and D. R. Worsnop (2000), Development of an aerosol mass spectrometer for size and composition analysis of submicron particles, *Aerosol Sci. Technol.*, *33*, 49–70, doi:10.1080/027868200410840.

Kleinman, L. I., et al. (2008), The time evolution of aerosol composition over the Mexico City plateau, *Atmos. Chem. Phys.*, *8*(6), 1559–1575, doi:10.5194/acp-8-1559-2008.

Koop, T., J. Bookhold, M. Shiraiwa, and U. Pöschl (2011), Glass transition and phase state of organic compounds: Dependency on molecular properties and implications for secondary organic aerosols in the atmosphere, *Phys. Chem. Chem. Phys.*, *13*, 19238–19255, doi:10.1039/c1cp22617g.

Kreidenweis, S. M., M. D. Petters, and P. J. DeMott (2008), Single parameter estimates of aerosol water content, *Environ. Res. Lett.*, *3*, doi:10.1088/1748-9326/3/3/035002.

Laborde, M., P. Mertes, P. Zieger, J. Dommen, U. Baltensperger, and M. Gysel (2012), Sensitivity of the Single Particle Soot Photometer to different black carbon types, *Atmos. Meas. Tech.*, *5*, 1031–1043, doi:10.5194/amt-5-1031-2012.

Lance, S., J. Medina, J. N. Smith, and A. Nenes (2006), Mapping the operation of the DMT continuous-flow CCN counter, *Aerosol Sci. Technol.*, *40*, 242–254, doi:10.1080/02786820500543290.

Liu, P., et al. (1995), Generating particle beams of controlled dimensions and divergence. 2. Experimental evaluation of particle motion in aerodynamic lenses and nozzle expansions, *Aerosol Sci. Technol.*, *22*, 314–324.

Liu, D., K. Prather, and S. Hering (2000), Variations in the size and chemical composition of nitrate-containing particles in Riverside, CA, *Aerosol. Sci. Tech.*, *33*, 71–86, doi:10.1080/027868200410859.

Lu, R., and R. Turco (1995), Air pollutant transport in a coastal environment—II. Three-dimensional simulations over Los Angeles Basin, *Atmos. Environ.*, *29*, 1499–1518.

Marcolli, C., and U. K. Krieger (2006), Phase changes during hygroscopic cycles of mixed organic/inorganic model systems of tropospheric aerosols, *J. Phys. Chem. A*, *110*, 1881–1893, doi:10.1021/jp0556759.

Massling, A., M. Stock, and A. Wiedensohler (2005), Diurnal, weekly, and seasonal variation of hygroscopic properties of submicrometer urban aerosol particles, *Atmos. Environ.*, *39*, 3911–3922, doi:10.1016/j.atmosenv.2005.03.020.

Massling, A., M. Stock, B. Wehner, Z. J. Wu, M. Hu, E. Bruggemann, T. Gnauk, H. Herrmann, and A. Wiedensohler (2009), Size segregated water uptake of the urban submicrometer aerosol in Beijing, *Atmos. Environ.*, *43*, 1578–1589, doi:10.1016/j.atmosenv.2008.06.003.

Massoli, P., et al. (2010), Relationship between aerosol oxidation level and hygroscopic properties of laboratory generated secondary organic aerosol (SOA) particles, *Geophys. Res. Lett.*, *37*, L24801, doi:10.1029/2010GL045258.

Meier, J., B. Wehner, A. Massling, W. Birmili, A. Nowak, T. Gnauk, E. Bruggemann, H. Herrmann, H. Min, and A. Wiedensohler (2009), Hygroscopic growth of urban aerosol particles in Beijing (China) during wintertime: a comparison of three experimental methods, *Atmos. Chem. Phys.*, *9*, 6865–6880, doi:10.5194/acp-9-6865-2009.

Metcalf, A. R., J. S. Craven, J. J. Ensberg, J. Brioude, W. Angevine, A. Sorooshian, H. T. Duong, H. H. Jonsson, R. C. Flagan, and J. H. Seinfeld (2012), Black carbon aerosol over the Los Angeles Basin during CalNex, *J. Geophys. Res. Atmos.*, *117*, doi:10.1029/2011JD017255.

Moffet, R. C., and K. A. Prather (2009), In-situ measurements of the mixing state and optical properties of soot with implications for radiative forcing estimates, *Proc. Natl. Acad. Sci. U. S. A.*, *106*, 11872–11877, doi:10.1073/pnas.0900040106.

Moore, K. F., Z. Ning, L. Ntziachristos, J. J. Schauer, and C. Sioutas (2007), Daily Variation in the properties of urban ultrafine aerosol—Part 1: Physical characterization and volatility, *Atmos. Environ.*, *41*, 8633–8646, doi:10.1016/j.atmosenv.2007.07.030.

Moore, R. H., and A. Nenes (2009), Scanning flow CCN analysis—A method for fast measurements of CCN spectra, *Aerosol Sci. Technol.*, *43*, 1192–1207, doi:10.1080/02786820903289780.

Moore, R. H., R. Bahreini, C. A. Brock, K. D. Froyd, J. Cozic, J. S. Holloway, A. M. Middlebrook, D. M. Murphy, and A. Nenes (2011), Hygroscopicity and composition of Alaskan Arctic CCN during April 2008, *Atmos. Chem. Phys.*, *11*, 11,807–11,825, doi:10.5194/acp-11-11807–2011.

Moteki, N., and Y. Kondo (2007), Effects of mixing state on black carbon measurements by laser-induced incandescence, *Aerosol Sci. Technol.*, *41*(4), 398–417, doi:10.1080/02786820701199728.

Murphy, S. M., et al. (2009), Comprehensive simultaneous shipboard and airborne characterization of exhaust from a modern container ship at sea, *Environ. Sci. Technol.*, *43*(13), 4626–4640, doi:10.1021/es802413j.

Neuman, J. A., et al. (2003), Variability in ammonium nitrate formation and nitric acid depletion with altitude and location over California, *J. Geophys. Res.*, *108*(D17), 4557, doi:10.1029/2003JD003616.

Quinn, P., et al. (2005), Impact of particulate organic matter on the relative humidity dependence of light scattering: A simplified parameterization, *Geophys. Res. Lett.*, *32*, 22, doi:10.1029/2005GL024322.

Pankow, J. F. (2003), Gas/particle partitioning of neutral and ionizing compounds to single and multi-phase aerosol particles. 1. Unified modeling framework, *Atmos. Environ.*, *37*(24), 3323–3333, doi:10.1016/S1352-2310(03)00346-7.

Pastor, S., J. Allen, L. Hughes, P. Bhave, G. Cass, and K. A. Prather (2003), Ambient single particle analysis in Riverside, California by aerosol time-of-flight mass spectrometry during the SCOS97-NARSTO, *Atmos. Environ.*, *37*, S239–S258, doi:10.1016/S13522310(03)00393-5.

Petters, M. D., and S. M. Kreidenweis (2007), A single parameter representation of hygroscopic growth and cloud condensation nucleus activity, *Atmos. Chem. Phys.*, *7*, 1961–1971, doi:10.5194/acp-7-1961-2007.

Petters, M. D., C. M. Carrico, S. M. Kreidenweis, A. J. Prenni, P. J. DeMott, J. L. Collett, and H. Moosmuller (2009), Cloud condensation nucleation activity of biomass burning aerosol, *J. Geophys. Res. Atmos.*, *114*, doi:10.1029/2009JD012353.

Pratt, K. A., and K. A. Prather (2009), Real-Time, Single-Particle Volatility, Size, and Chemical Composition Measurements of Aged Urban Aerosols, *Environ. Sci. Technol.*, *43*, 8276–8282, doi:10.1021/es902002t.

Pratt, K. A., et al. (2009a), Development and characterization of an aircraft aerosol time-of-flight mass spectrometer. *Anal. Chem.*, *81*, 1792–1800, doi:10.1021/ac801942r.

Pratt, K. A., et al. (2009b), In situ detection of biological particles in cloud ice-crystals, *Nat. Geosci.*, *2*, 398–401.

Pratt, K. A., et al. (2011), Flight-based chemical characterization of biomass burning aerosols within two prescribed burn smoke plumes, *Atmos. Chem. Phys.*, *11*, 12549–12565, doi:10.5194/acp-11-12549-2011.

Prenni, A., P. DeMott, S. Kreidenweis, D. Sherman, L. Russell, and Y. Ming (2001), The effects of low molecular weight dicarboxylic acids on cloud formation, *J. Phys. Chem. A*, *105*, 11240–11248.

Qin, X, K. A. Pratt, L. G. Shields, S. M. Toner, and K. A. Prather (2012), Seasonal comparisons of single-particle chemical mixing state in Riverside, CA. *Atmos. Environ*, *59*, 587–596, doi:10.1016/j.atmosenv.2012.05.032.

Russell, S. C. (2009), Microorganism characterization by single particle mass spectrometry, *Mass Spectrom. Rev.*, *28*, 376–387, doi:10.1002/mas.20198.

Roberts, G. C., and A. Nenes (2005), A continuous-flow streamwise thermal-gradient CCN chamber for atmospheric measurements, *Aerosol Sci. Technol.*, *39*, 206–221, doi:10.1080/027868290913988.

Rose, D., A. Nowak, P. Achtert, A. Wiedensohler, M. Hu, M. Shao, Y. Zhang, M. Andreae, and U. Pöschl (2010), Cloud condensation nuclei in polluted air and biomass burning smoke near the megacity Guangzhou, China—Part 1: Size-resolved measurements and implications for the modeling of aerosol particle hygroscopicity and CCN activity, *Atmos. Chem. Phys.*, *10*, 3365–3383, doi:10.5194/acp-10-3365-2010.

Sareen, N., A. N. Schwier, T. L. Lathem, A. Nenes, and V. F. McNeill (2012), Surfactants from the gas phase may promote cloud droplet formation, *Proc. Natl. Acad. Sci. U. S. A.*, doi:10.1073/pnas.1204838110.

Saxena, P., L. M. Hildemann, P. H. McMurry, and J. H. Seinfeld (1995), Organics alter hygroscopic behavior of atmospheric particles, *J. Geophys. Res. Atmos.*, *100*, 18755–18770.

Schwarz, J. P., et al. (2006), Single-particle measurements of midlatitude black carbon and light-scattering aerosols from the boundary layer to the lower stratosphere, *J. Geophys. Res.*, *111*, D16207, doi:10.1029/2006JD007076.

Seinfeld, J. H., and S. N. Pandis (2006), Atmospheric Chemistry and Physics: From Air Pollution to Climate Change, pp. 469, John Wiley & Sons, Hoboken, NJ, USA.

Shields, L. G., D. T. Suess, and K. A. Prather (2007), Determination of single particle mass spectral signatures from heavy-duty diesel vehicle emissions for PM2.5 source apportionment, *Atmos. Environ.*, *41*, 3841–3852, doi:10.1016/j.atmosenv.2007.01.025.

Shields, L. G., X. Y. Qin, S. M. Toner, and K. A. Prather (2008), Detection of ambient ultrafine aerosols by single particle techniques during the SOAR 2005 campaign, *Aeorosol. Sci. Tech.*, *42*(8), 674–684, doi:10.1080/02786820802227378.

Shinozuka, Y., et al. (2009), Aerosol optical properties relevant to regional remote sensing of CCN activity and links to their organic mass fraction: airborne observations over Central Mexico and the US West Coast during MILAGRO/INTEX-B, *Atmos. Chem. Phys.*, *9*, 6727–6742, doi:10.5194/acp-9-6727-2009.

Shiraiwa, M., M. Ammann, T. Koop, and U. Pöschl (2011), Gas uptake and chemical aging of semisolid organic aerosol particles, *Proc. Natl. Acad. Sci. U. S. A.*, *108*(27), 11003–11008, doi:10.1073/pnas.1103045108.

Shiraiwa, M., C. Pfrang, T. Koop, and U. Pöschl (2012), Kinetic multi-layer model of gas-particle interactions in aerosols and clouds (KM-GAP): Linking condensation, evaporation and chemical reactions of organics, oxidants and water, *Atmos. Chem. Phys.*, *12*(5), 2777–2794, doi:10.5194/acp-12-2777-2012.

Silva, P. J., et al. (1999), Size and chemical characterization of individual particles resulting from biomass burning of local Southern California species, *Environ. Sci. Technol.*, *33*, 3068–3076.

Slowik, J. G., et al. (2007), An inter-comparison of instruments measuring black carbon content of soot particles, *Aerosol Sci. Technol.*, *41*(3), 295–314, doi:10.1080/02786820701197078.

Smith, M. L., M. Kuwata, and S. T. Martin (2011), Secondary organic material produced by the dark ozonolysis of α-pinene minimally affects the deliquescence and efflorescence of ammonium sulfate, *Aerosol Sci. Technol.*, *45*, 244–261, doi:10.1080/02786826.2010.532178, http://dx.doi.org/10.1080/ 02786826.2010.532178.

Sodeman, D. A., S. M. Toner, and K. A. Prather (2005), Determination of single particle mass spectral signatures from light-duty vehicle emissions, *Environ. Sci. Technol.*, *39*, 4569–4580, doi:10.1021/es0489947.

Song, X. H., et al. (1999), Classification of single particles analyzed by ATOFMS using an artificial neural network, ART-2A, *Anal. Chem.*, *71*, 860–865.

Song, M., C. Marcolli, U. K. Krieger, A. Zuend, and T. Peter (2012a), Liquid-liquid phase separation and morphology of internally-mixed dicarboxylic acids/ammonium sulfate/water particles, *Atmos. Chem. Phys.*, *12*, 2691–2712, doi:10.5194/acp-12-2691-2012.

Song, M., C. Marcolli, U. K. Krieger, A. Zuend, and T. Peter (2012b), Liquid-liquid phase separation in aerosol particles: Dependence on O:C, organic functionalities, and compositional complexity, *Geophys. Res. Lett. 39*, L19801, doi:10.1029/2012gl052807.

Sorooshian, A., F. J. Brechtel, Y. L. Ma, R. J. Weber, A. Corless, R. C. Flagan, and J. H. Seinfeld (2006), Modeling and characterization of a particle-into-liquid sampler (PILS), *Aerosol Sci. Technol.*, *40*, 396–409, doi:10.1080/02786820600632282.

Sorooshian, A., S. P. Hersey, F. J. Brechtel, A. Corless, R. C. Flagan, and J. H. Seinfeld (2008), Rapid size-resolved aerosol hygroscopic growth measurements: differential aerosol sizing and hygroscopicity spectrometer probe (DASH-SP), *Aerosol Sci. Technol.*, *42*, 445–464, doi:10.1080/02786820802178506.

Spencer, M. T., and K. A. Prather (2006), Using ATOFMS to determine OC/EC mass fractions in particles, *Aerosol Sci. Technol.*, *40*, 585–594, doi:10.1080/02786820600729138.

Stephens, M., N. Turner, and J. Sandberg (2003), Particle identification by laser-induced incandescence in a solid-state laser cavity, *Appl. Opt.*, *42*(19), 3726–3736, doi:10.1364/AO.42.003726.

Sullivan, A. P., R. E. Peltier, C. A. Brock, J. A. de Gouw, J. S. Holloway, C. Warneke, A. G. Wollny, and R. J. Weber (2006), Airborne measurements of carbonaceous aerosol soluble in water over northeastern United States: Method development and an investigation into water-soluble organic carbon sources, *J. Geophys. Res.*, *111*, D23S46, doi:10.1029/2006JD007072.

Sun, J., Q. Zhang, M. R. Canagaratna, Y. Zhang, N. L. Ng, Y. Sun, J. T. Jayne, X. Zhang, X. Zhang, and D. R. Worsnop (2009), Highly time- and size-resolved characterization of submicron aerosol particles in Beijing using an aerodyne aerosol mass spectrometer, *Atmos. Environ.*, *44*, 131–140, doi:10.1016/j.atmosenv.2009.03.020.

Swietlicki, E., et al. (2008), Hygroscopic properties of submicrometer atmospheric aerosol particles measured with H-TDMA instruments in various environments: A review, *Tellus B*, *60*, 432–469, doi:10.3402/tellusb.v60i3.16936.

Tiitta, P., et al. (2010), Roadside aerosol study using hygroscopic, organic and volatility TDMAs: Characterization and mixing state, *Atmos. Environ.*, *44*, 976–986, doi:10.1016/j.atmosenv.2009.06.021.

Toner, S. M., D. A. Sodeman, and K. A. Prather (2006), Single particle characterization of ultrafine and accumulation mode particles from heavy duty diesel vehicles using aerosol time-of-flight mass spectrometry, *Environ. Sci. Technol.*, *40*, 3912–3921, doi:10.1021/es051455x.

Tong, H. J., J. P. Reid, D. L. Bones, B. P. Luo, and U. K. Krieger (2011), Measurements of the timescales for the mass transfer of water in glassy aerosol at low relative humidity and ambient temperature, *Atmos. Chem. Phys.*, *11*, 4739–4754, doi:10.5194/acp-11-4739-2011.

Turpin, B., and J. Huntzicker (1991), Secondary formation of organic aerosol in the Los Angeles Basin—A descriptive analysis of organic and elemental carbon concentrations, *Atmos. Environ.*, *25*, 207–215, doi:10.1016/0960-1686(91)90291-E.

Virtanen, A., et al. (2010), An amorphous solid state of biogenic secondary organic aerosol particles, *Nature*, *467*, 824–827, doi:10.1038/nature09455.

Watson, J. G., J. C. Chow, Z. Q. Lu, E. M. Fujita, D. H. Lowenthal, D. R. Lawson, and L. L. Ashbaugh (1994), Chemical mass-balance source apportionment of Pm(10) during the Southern California Air-Quality Study, *Aerosol Sci. Technol.*, *21*, 1–36.

Wex, H., G. McFiggans, S. Henning, and F. Stratmann (2010), Influence of the external mixing state of atmospheric aerosol on derived CCN number concentrations, *Geophys. Res. Lett.*, *37*, doi:10.1029/2010GL043337.

Wonaschütz, A., S. P. Hersey, A. Sorooshian, J. Craven, A. R. Metcalf, R. C. Flagan, and J. H. Seinfeld (2011), Impact of a large wildfire on water-soluble organic aerosol in a major urban setting: The 2009 station fire in Los Angeles County, *Atmos. Chem. Phys.*, *11*, 8257–8270, doi:10.5194/acp-11-8257-2011.

Wu, J., D. L. Nofziger, J. Warren, and J. Hattey (2003), Estimating ammonia volatilization from swine-effluent droplets in sprinkle irrigation, *Soil Sci. Soc. Am. J.*, *67*(5), 1352–1360, doi:10.2136/sssaj2003.1352.

You, Y., et al. (2012), Images reveal that atmospheric particles can undergo liquid-liquid phase separations, *Proc. Natl. Acad. Sci. U. S. A.*, *109*, 13188–13193, doi:10.1073/pnas.1206414109.

Zhang, Q., M. R. Canagaratna, J. T. Jayne, D. R. Worsnop, and J. L. Jimenez (2005a), Time- and size-resolved chemical composition of submicron particles in Pittsburgh: Implications for aerosol sources and processes, *J. Geophys. Res.*, *110*, doi:10.1029/2004JD004649.

Zhang, Q., D. R. Worsnop, M. R. Canagaratna, and J. L. Jimenez (2005b), Hydrocarbon-like and oxygenated organic aerosols in Pittsburgh: Insights into sources and processes of organic aerosols, *Atmos. Chem. Phys.*, *5*, 3289–3311, doi:10.5194/acp-5-3289-2005.

Zhang, Q., et al. (2007), Ubiquity and dominance of oxygenated species in organic aerosols in anthropogenically-influenced Northern Hemisphere midlatitudes, *Geophys. Res. Lett.*, *34*, L13801, doi:13810.11029/12007GL029979.

Zobrist, B., V. Soonsin, B. P. Luo, U. K. Krieger, C. Marcolli, T. Peter, and T. Koop (2011), Ultra-slow water diffusion in aqueous sucrose glasses, *Phys. Chem. Chem. Phys.*, *13*, 3514–3526, doi:10.1039/c0cp01273d.

Zuend, A., and J. H. Seinfeld (2012), Modeling the gas-particle partitioning of secondary organic aerosol: the importance of liquid-liquid phase separation, *Atmos. Chem. Phys.*, *12*, 3857–3882, doi:10.5194/acp-12-3857-2012.

Zuend, A., C. Marcolli, B. P. Luo, and T. Peter (2008), A thermodynamic model of mixed organic-inorganic aerosols to predict activity coefficients, *Atmos. Chem. Phys.*, *8*, 4559–4593, doi:10.5194/acp-8-4559-2008.

Zuend, A., C. Marcolli, T. Peter, and J. H. Seinfeld (2010), Computation of liquid-liquid equilibria and phase stabilities: Implications for RH-dependent gas/particle partitioning of organic-inorganic aerosols, *Atmos. Chem. Phys.*, *10*(16), 7795–7820, doi:10.5194/acp-10-7795-2010.

Zuend, A., C. Marcolli, A. M. Booth, D. M. Lienhard, V. Soonsin, U. K. Krieger, D. O. Topping, G. McFiggans, T. Peter, and J. H. Seinfeld (2011), New and extended parameterization of the thermodynamic model AIOMFAC: calculation of activity coefficients for organic-inorganic mixtures containing carboxyl, hydroxyl, carbonyl, ether, ester, alkenyl, alkyl, and aromatic functional groups, *Atmos. Chem. Phys.*, *11*, 9155–9206, doi:10.5194/acp-11-9155-2011.